NASA
Technical
Paper
2398
C.2
March 1985

Noise Transmission Loss of a Rectangular Plate in an Infinite Baffle

Louis A. Roussos

NASA

NASA Technical Paper 2398

1985

Noise Transmission Loss of a Rectangular Plate in an Infinite Baffle

Louis A. Roussos

Langley Research Center
Hampton, Virginia

NASA
National Aeronautics
and Space Administration

Scientific and Technical Information Branch

Summary

An improved analytical procedure has been developed that allows for an efficient solution of the finite plate noise transmission problem. Both isotropic and symmetrically laminated composite plates are considered. The plate is modeled with classic thin-plate theory and is assumed to be simply supported on all four sides. The incident acoustic pressure is modeled as a plane wave impinging on the plate at an arbitrary angle. The reradiated pressure is assumed to be negligible compared with the blocked pressure, and the plate vibrations are calculated by a normal-mode approach. A Green's function integral equation is used to link the plate vibrations to the transmitted far-field sound waves, and transmission loss is calculated from the ratio of incident to transmitted acoustic powers. The result is a versatile research and engineering analysis tool that not only enables the determination of which modes are dominating the noise transmission but also allows for the problem to be broken down into its component parts. This includes determining what the modal behavior is, such as coupling between the incident noise and the plate vibrations, the plate resonance behavior, and the coupling between the plate vibrations and the transmitted noise. The effect of varying the angle of incidence and the far-field directivity can also be determined from the analytical model. The analysis approach was specifically developed to study noise transmission into aircraft, although it should be equally applicable to sound transmission through building walls, floors, and windows.

Introduction

Noise transmission is an important consideration in the design of many structures, such as building walls and floors, ship hulls, and aircraft sidewalls. Consequently, a variety of analytical models have been developed over the years to predict the noise transmission characteristics of walls. These analytical models may be further classified as either high-frequency-noise or low-frequency-noise models.

In high-frequency noise, the dimensions of the walls are very large compared with the relatively small sound wavelengths, so the wall can be modeled analytically as infinite in extent. This is referred to as "infinite-panel theory." Noise transmission analytical models based on infinite-panel theory have been extensively developed in the past (refs. 1 to 4) and dealt with such features as single-layer and multilayer panels, oblique-incidence and random-incidence noise, and isotropic, orthotropic, and anisotropic panels.

In low-frequency noise, the dimensions of the transmitting wall are comparable with the large sound wavelengths, so that boundary effects are important. In this approach, the wall is usually modeled as a rectangular plate simply supported in an infinite baffle. This model is especially desirable because it exhibits many of the same noise transmission phenomena that occur in more complicated structures and that are more easily studied in this idealized problem. However, noise transmission models for this problem have been much less studied. Most of the past work on this problem has been concentrated on solving for the radiated noise or the radiation efficiency of the plate vibrations (refs. 5 to 11). Only a few investigators have looked at the entire problem: the incident noise, the plate vibrations, and the transmitted noise, and all these studies ended up with very limited and mainly qualitative results (refs. 12 to 16). This was invariably due to either the simplifying assumptions limiting the applicability of the analysis or, in the opposite case, the lack of assumptions causing the mathematics to be very complicated.

In this paper, an improved analytical model that allows for the efficient calculation of the low-frequency-noise transmission characteristics of a rectangular plate simply supported in an infinite baffle is developed. The first section of the paper contains the derivation of the analytical model equations. First, the equation for the transmission loss of the finite plate is derived. The paper starts with the basic equations describing the incident noise and the plate vibrations and takes a step-by-step approach and derives the equations for incident intensity, incident acoustic power, plate velocity, transmitted pressure, transmitted intensity, and transmitted acoustic power. Transmission loss is then calculated from the ratio of transmitted to incident acoustic power. This ratio is called the transmission coefficient. The general solution for transmission loss includes the response of a large number of modes. To investigate the response of these individual modes, equations are derived describing the component parts of the transmission coefficient of each mode.

The transmission coefficient is factored into the ratio of transmitted acoustic power to mean-square plate velocity and the ratio of mean square plate velocity to incident acoustic power. This latter ratio is then broken down into two more parts with equations being derived for the frequency response of the plate vibrations and the frequency response of the exciting acoustic pressure. With the analytical model equations having been derived for an isotropic plate, an extension of the model to handle midplane symmetric composite panels is briefly discussed.

In the second section of the paper, results of sample calculations using the analytical model are shown. First, polar plots of far-field transmitted intensity are shown for both low-frequency-noise and high-frequency-noise transmission. Next are shown the results of sample calculations of transmission loss. The finite-panel theory is compared with infinite-panel theory, and the variation of transmission loss with the incidence angles is shown. Then, results are shown of a modal study of the noise transmission at 600 Hz as an example of the use of the analytical model as a diagnostic tool. The model is used to determine which modes are dominating the transmission at this frequency and whether this transmission is due to coupling between the incident noise and the plate vibrations, to plate resonance behavior, or to coupling between the plate vibrations and the space into which the plate is transmitting. Results are also presented that demonstrate the applicability of the analytical model for studying the effect of fiber orientation on the transmission loss of midplane symmetric composite panels.

Symbols

a	length of plate, m
b	width of plate, m
C_D	equivalent viscous damping constant, N-sec/m
c	speed of sound, m/sec
D	bending stiffness for an isotropic plate, N-m
$D_{11}, D_{12}, D_{16}, D_{22}, D_{26}, D_{66}$	bending stiffnesses for an anisotropic plate, N-m
E_{11}, E_{22}	orthotropic elastic moduli in a composite-tape ply parallel and perpendicular to the fibers, respectively, Pa
f	frequency, Hz
f_{mn}	resonant frequency of a mode, Hz
G_{12}	shear modulus for composite-tape ply, Pa
I_m	dummy variable which is a function of m and is equal to the integral over ξ in the Rayleigh integral
$\bar{I}_m$	dummy variable which is a function of m and is equal to the integral over ξ in the equation for the generalized forcing pressure
I_n	dummy variable which is a function of n and is equal to the integral over η in the Rayleigh integral
$\bar{I}_n$	dummy variable which is a function of n and is equal to the integral over η in the equation for the generalized forcing pressure
I_t	transmitted intensity, N/m-sec
i	$= \sqrt{-1}$

k	wave number, ω/c, rad/m
m	number of half-wavelengths in direction parallel to length of plate
m_p	mass per unit area of plate, kg/m^2
n	number of half-wavelengths in direction parallel to width of plate
P_i	amplitude of incident pressure, Pa
p_i	incident pressure, Pa
p_{mn}	generalized forcing pressure, Pa
p_r	reflected pressure, Pa
p_t	transmitted pressure, Pa
r	radial distance from a point in the far field to the center of the plate, m
r'	radial distance from a point in the far field to an arbitrary point on the plate, m
sgn( )	sign (either 1 or -1) of the variable in parentheses
t	time, sec
TL	transmission loss, dB
V_{mn}	generalized plate velocity, m/sec
W	amplitude of displacement, m
w	transverse plate displacement, m
W_{mn}	generalized displacement, m
x, y, z	Cartesian coordinates for a point in the far field (z is perpendicular to the plate), m
ς	critical damping ratio
θ	polar angle location of a point in the far field, rad
θ_i	polar incidence angle, rad
ν_{12}	composite-tape-ply Poisson's ratios
ξ, η	coordinates for a point on the plate, m
Π_i	incident acoustic power, W
Π_t	transmitted acoustic power, W
ρ	mass density of air, kg/m^3
τ	transmission coefficient
τ_{mn}	transmission coefficient for a mode
ϕ	azimuthal angle location of a point in the far field, rad
ϕ_i	azimuthal incidence angle, rad
ω	circular frequency, rad/sec
∇	del operator

Description of the Analytical Model

Incident Noise and Plate Vibration

With classic thin-plate theory, the equation of motion governing the bending vibrations of an isotropic plate is

$$D\,\nabla^4 w + C_D w_{,t} + m_p w_{,tt} = p_i(\xi,\eta,t) + p_r(\xi,\eta,t) - p_t(\xi,\eta,t) \tag{1}$$

where

$$\nabla^4 = \partial^4/\partial\xi^4 + 2\partial^4/\partial\xi^2\,\partial\eta^2 + \partial^4/\partial\eta^4$$

A comma denotes the partial differentiation with respect to the subscript; p_i, p_r, and p_t are the incident, reflected, and transmitted pressures; and the geometry of the coordinate system is given in figure 1. These three pressures can be rewritten as the sum of the blocked pressure (the pressure that occurs on the incident side when the plate is considered as a rigid wall) and the reradiated pressure (the pressure solely due to the plate vibrating). Because the reradiated pressure is an unknown function of the plate displacement w, the solution of equation (1) is very complicated. This is the main reason past investigators have been unable to arrive at effective, usable results. In order to arrive at an accurate solution while avoiding this complication, the present analysis assumes that the reradiated pressure is negligible compared with the blocked pressure in the equation of motion for the plate. With the infinite-panel theory, this assumption results in errors of less than 1 dB for transmission loss values of 6 dB or more. Thus, the assumption allows an accurate solution to be obtained over a large frequency range and gives invalid answers only for frequencies near the plate fundamental resonant frequency.

Rewriting the equation of motion with only the blocked pressure as the forcing function results in

$$D\,\nabla^4 w + C_D w_{,t} + m_p w_{,tt} = p_b(\xi,\eta,t) \tag{2}$$

where the blocked pressure p_b is twice the incident pressure ($p_b(\xi,\eta,t) = 2p_i(\xi,\eta,t)$). Now the incident pressure is assumed to be an obliquely incident traveling plane wave given by

$$p_i(\xi,\eta,t) = P_i \exp\left[i\left(\omega t - k\xi\sin\theta_i\cos\phi_i - k\eta\sin\theta_i\sin\phi_i\right)\right] \tag{3}$$

where the amplitude P_i of the incident pressure is assumed to be a real constant, an assumption that results in no loss of generality. The relationship between the incidence angles and the coordinate axes is shown in figure 1. At this point the incident intensity and the incident acoustic power can be calculated. Since the incident noise is a plane wave, it is well known the intensity is given by $P_i^2/2\rho c$ (ref. 17). The intensity incident on the plate is the amount of the intensity that is normal to the plate. Thus, the incident intensity I_i is given by

$$I_i = \left(P_i^2\cos\theta_i\right)/2\rho c \tag{4}$$

The incident acoustic power Π_i is simply given by the incident intensity multiplied by the area it acts on, that is, the area of the plate. Thus, Π_i is given by

$$\Pi_i = \left(P_i^2 ab\cos\theta_i\right)/2\rho c \tag{5}$$

The steady-state solution for the plate vibration displacement is the only part of the solution of concern in predicting noise transmission; since the forcing pressure is harmonic, the steady-state plate displacement will be harmonic such that

$$w(\xi, \eta, t) = W(\xi, \eta) \exp(i\omega t) \tag{6}$$

Substituting equations (3) and (6) into (2) and dividing through by $\exp(i\omega t)$ gives

$$D\,\nabla^4 W(\xi, \eta) + iC_D\omega W(\xi, \eta) - m_p\omega^2 W(\xi, \eta) = 2P_i \exp\left[-ik \sin\theta_i \left(\xi \cos\phi_i + \eta \sin\phi_i\right)\right] \tag{7}$$

The finiteness of the plate is now taken into consideration. The plate is assumed to be rectangular and simply supported on all four sides. The solution of equation (7) can be obtained by using the method of eigenfunctions (ref. 18). Homogeneously solving equation (7) by separation of variables and applying simple-support boundary conditions gives

$$W(\xi, \eta) = \sum_{m=1}^{\infty} \sum_{n=1}^{\infty} W_{mn} \sin\left(\frac{m\pi\xi}{a}\right) \sin\left(\frac{n\pi\eta}{b}\right) \tag{8}$$

Since the steady-state solution (see eq. (6)) must also satisfy the boundary conditions, equation (8) can be used for the spatial part of the steady-state solution so long as the spatial part of the forcing pressure can also be represented as an infinite series of the eigenfunctions. For the case at hand, the forcing pressure can be so represented, and the result is

$$2P_i \exp\left[-ik \sin\theta_i \left(\xi \cos\phi_i + \eta \sin\phi_i\right)\right] = \sum_{m=1}^{\infty} \sum_{n=1}^{\infty} p_{mn} \sin\left(\frac{m\pi\xi}{a}\right) \sin\left(\frac{n\pi\eta}{b}\right) \tag{9}$$

where p_{mn}, the generalized forcing pressure, is given by

$$p_{mn} = \frac{8P_i}{ab} \int_{\xi=0}^{a} \int_{\eta=0}^{b} \exp\left[-ik \sin\theta_i \left(\xi \cos\phi_i + \eta \sin\phi_i\right)\right] \sin\left(\frac{m\pi\xi}{a}\right) \sin\left(\frac{n\pi\eta}{b}\right) d\eta\, d\xi \tag{10}$$

The generalized displacement W_{mn} can now be obtained by substituting equations (8) and (9) into equation (7) and obtaining

$$W_{mn} = \frac{p_{mn}}{m_p \left[\omega_{mn}^2 - \omega^2 + (iC_D\omega/m_p)\right]} \tag{11}$$

where

$$\omega_{mn}^2 = (2\pi f_{mn})^2 = \frac{D\pi^4}{m_p} \left(\frac{m^2}{a^2} + \frac{n^2}{b^2}\right)^2 \tag{12}$$

The integration in equation (10) can be done in closed form to obtain the generalized forcing pressure for each mode

$$p_{mn} = 8P_i \bar{I}_m \bar{I}_n \tag{13}$$

where

$$\bar{I}_m = \begin{cases} -\frac{i}{2}\operatorname{sgn}(\sin\theta_i \cos\phi_i) & \left((m\pi)^2 = [\sin\theta_i \cos\phi_i(\omega a/c)]^2\right) \\ \dfrac{m\pi\{1-(-1)^m \exp[-i\sin\theta_i \cos\phi_i(\omega a/c)]\}}{(m\pi)^2 - [\sin\theta_i \cos\phi_i(\omega a/c)]^2} & \left((m\pi)^2 \neq [\sin\theta_i \cos\phi_i(\omega a/c)]^2\right) \end{cases}$$

$$\bar{I}_n = \begin{cases} -\frac{i}{2}\operatorname{sgn}(\sin\theta_i \sin\phi_i) & \left((n\pi)^2 = [\sin\theta_i \sin\phi_i(\omega b/c)]^2\right) \\ \dfrac{n\pi\{1-(-1)^n \exp[-i\sin\theta_i \sin\phi_i(\omega b/c)]\}}{(n\pi)^2 - [\sin\theta_i \sin\phi_i(\omega b/c)]^2} & \left((n\pi)^2 \neq [\sin\theta_i \sin\phi_i(\omega b/c)]^2\right) \end{cases}$$

Thus, the solution for the plate vibrations is complete.

Transmitted Noise and Transmission Loss

The plate vibrations cause reradiated pressure to be transmitted by the plate. The equation relating plate velocity to the transmitted pressure can be derived from a Green's function formulation (ref. 19) starting from the basic fluid flow conservation equations together with the Kirchoff-Helmholtz method of integration. The resulting equation for transmitted pressure is commonly known as the Rayleigh integral and is given by

$$p_t(r,\theta,\phi) = \int_{\xi'=-a/2}^{a/2} \int_{\eta'=-b/2}^{b/2} \frac{i\rho\omega}{2\pi r'} \frac{\partial w(\xi',\eta',t)}{\partial t} \exp(-i\omega r'/c)\, d\xi'\, d\eta' \tag{14}$$

where

$$\xi' = \xi - \frac{a}{2}$$

$$\eta' = \eta - \frac{b}{2}$$

and

$$r' = \sqrt{(x-\xi')^2 + (y-\eta')^2 + z^2}$$

The transmission geometry is given in figure 2. Since

$$r = \sqrt{x^2 + y^2 + z^2}$$

$$x = r\sin\theta\cos\phi$$

and

$$y = r\sin\theta\sin\phi$$

the equation for r' can be rewritten as

$$r' = r\sqrt{1 - \frac{2\sin\theta\cos\phi}{r}\xi' + \left(\frac{\xi'}{r}\right)^2 - \frac{2\sin\theta\sin\phi}{r}\eta' + \left(\frac{\eta'}{r}\right)^2} \tag{15}$$

The integral in equation (14) must be evaluated numerically. However, a closed-form solution for this integral can be obtained in the far field. In the far field, the following approximations are valid (ref. 17):

$$\frac{1}{r'} \approx \frac{1}{r}$$

and

$$\exp(-i\omega r'/c) \approx \exp\left[-i(\omega/c)r\left(1 - \frac{\sin\theta\cos\phi}{r}\xi' - \frac{\sin\theta\sin\phi\eta'}{r}\right)\right]$$

Thus, the far-field transmitted pressure is given by

$$p_t(r,\theta,\phi) = \frac{i\omega\rho}{2\pi r}\int_{-a/2}^{a/2}\int_{-b/2}^{b/2}\frac{\partial w(\xi',\eta',t)}{\partial t}\exp\left[-ikr\left(1 - \frac{\sin\theta\cos\phi}{r}\xi' - \frac{\sin\theta\sin\phi}{r}\eta'\right)\right]\,d\eta'\,d\xi' \tag{16}$$

Plate motion is assumed to be continuous through the thickness of the plate so that $w(\xi,\eta,t)$ is given by equations (6) and (8). Thus,

$$\frac{\partial w(\xi,\eta,t)}{\partial t} = i\omega\left[\sum_{m=1}^{\infty}\sum_{n=1}^{\infty}W_{mn}\sin\left(\frac{m\pi\xi}{a}\right)\sin\left(\frac{n\pi\eta}{b}\right)\right]\exp(i\omega t) \tag{17}$$

Substituting equation (17) into (16) allows a closed-form solution to be obtained for the Rayleigh integral as follows:

$$p_t(r,\theta,\phi) = \frac{-\omega^2\rho ab}{2\pi r}\exp\left\{i\omega\left[t - \frac{r}{c} - \frac{\sin\theta}{2c}(a\cos\phi + b\sin\phi)\right]\right\}\sum_{m=1}^{\infty}\sum_{n=1}^{\infty}W_{mn}I_mI_n \tag{18}$$

where

$$I_m = \begin{cases} -\frac{i}{2}\mathrm{sgn}(\sin\theta\cos\phi) & \left((m\pi)^2 = [\sin\theta\cos\phi(\omega a/c)]^2\right) \\ \dfrac{m\pi\left\{1-(-1)^m\exp\left[i\sin\theta\cos\phi(\omega a/c)\right]\right\}}{(m\pi)^2 - [\sin\theta\cos\phi(\omega a/c)]^2} & \left((m\pi)^2 \neq [\sin\theta\cos\phi(\omega a/c)]^2\right) \end{cases}$$

$$I_n = \begin{cases} -\frac{i}{2}\mathrm{sgn}(\sin\theta\sin\phi) & \left((n\pi)^2 = [\sin\theta\sin\phi(\omega b/c)]^2\right) \\ \dfrac{n\pi\left\{1-(-1)^n\exp\left[i\sin\theta\sin\phi(\omega b/c)\right]\right\}}{(n\pi)^2 - [\sin\theta\sin\phi(\omega b/c)]^2} & \left((n\pi)^2 \neq [\sin\theta\sin\phi(\omega b/c)]^2\right) \end{cases}$$

Now, to calculate the far-field intensity, the far-field acoustic particle velocity must first be calculated. The equation for the velocity vector $\mathbf{u}(r,\theta,\phi)$ is

$$\mathbf{u}(r,\theta,\phi) = \frac{i}{\omega\rho}\nabla p_t(r,\theta,\phi) = u_r\mathbf{i}_r + u_\theta\mathbf{i}_\theta + u_\phi\mathbf{i}_\phi \tag{19}$$

where $\mathbf{i}_r, \mathbf{i}_\theta$, and $\mathbf{i}_\phi$ are the unit vectors in the r-, θ-, and ϕ-directions; u_r, u_θ, and u_ϕ are the velocity components in those directions; and

$$\nabla = \frac{\partial}{\partial r}\mathbf{i}_r + \frac{1}{r}\frac{\partial}{\partial\theta}\mathbf{i}_\theta + \frac{1}{r\sin\theta}\frac{\partial}{\partial\phi}\mathbf{i}_\phi$$

In the far field, r will be large so that the radial component of velocity will be much larger than the components of velocity in the $\mathbf{i}_\theta$- and $\mathbf{i}_\phi$-directions. Thus, the far-field velocity is approximated by the

scalar u_r. Substituting equation (18) into (19) and neglecting the $1/r^2$ terms compared with the $1/r$ terms gives

$$u_r = p_t/\rho c \tag{20}$$

If far-field pressure and velocity are known, the far-field transmitted intensity I_t can be calculated by substituting equation (20) into the basic definition of I_t as follows:

$$I_t = \frac{1}{2}\mathrm{Re}\left[p_t(r,\theta,\phi)u_r^*(r,\theta,\phi)\right] \tag{21}$$

where Re [ ] denotes the real part and the asterisk denotes the complex conjugate. The result of this is

$$I_t = |p_t(r,\theta,\phi)|^2/2\rho c \tag{22}$$

If we substitute for $p_t(r,\theta,\phi)$ from equation (18), the equation for I_t becomes

$$I_t = \frac{\rho}{2c}\left(\frac{4P_i ab}{\pi r m_p}\right)^2 \left|\sum_{m=1}^{\infty}\sum_{n=1}^{\infty} Q_{mn}\right|^2 \tag{23}$$

where

$$Q_{mn} = \frac{I_m I_n \bar{I}_m \bar{I}_n}{(f_{mn}/f)^2 - 1 + 2i\varsigma f_{mn}/f} \tag{24}$$

and

$$\varsigma = \frac{C_D}{2m_p\omega_{mn}}$$

The transmitted acoustic power Π_t can now be calculated by integrating the transmitted intensity over a far-field hemisphere such that

$$\Pi_t = \int_{\phi=0}^{2\pi}\int_{\theta=0}^{\pi/2} I_t r^2 \sin\theta \; d\theta \; d\phi \tag{25}$$

This equation must be integrated numerically. Simpson's one-third rule (ref. 20) was used in the calculations that were done in conjunction with the present study. Finally, transmission loss (TL) is calculated from

$$\mathrm{TL} = 10\log\left(1/\tau\right) \tag{26}$$

where the transmission coefficient τ is given by

$$\tau = \Pi_t/\Pi_i \tag{27}$$

Modal Components of Transmission

Presented here is a derivation of equations which can be used to study an individual mode's noise transmission characteristics. They can be used for both the characteristics of the total problem and the characteristics of the different components of the problem.

First of all, for the total noise transmission response of a single mode, the following single-mode equation for the transmission coefficient is used:

$$\tau_{mn} = \left(\frac{4\rho}{\pi m_p}\right)^2 \frac{4ab}{\cos\theta_i} \int_{\theta=0}^{\pi/2} \int_{\phi=0}^{\pi/2} \left| \frac{I_m I_n \bar{I}_m \bar{I}_n}{(f_{mn}/f)^2 - 1 + 2i\zeta f_{mn}/f} \right|^2 d\phi \, \sin\theta \, d\theta \tag{28}$$

where, because of symmetry, integration over ϕ is necessary only from 0 to $\pi/2$. This result can be used to determine the frequency at which a mode is transmitting the most noise. To determine what part of the total noise transmission is the primary cause of the transmission, the transmission coefficient is divided into the following two multiplicative factors: the acoustic power transmitted divided by mean-square velocity $\left(\Pi_t/|V_{mn}|^2\right)$ and the mean-square velocity divided by incident acoustic power $\left(|V_{mn}|^2/\Pi_i\right)$, where V_{mn} is the generalized plate modal velocity and is equal to $i\omega W_{mn}$. The equations corresponding to these factors are

$$\Pi_t/|V_{mn}|^2 = \int_{\phi=0}^{\pi/2} \int_{\theta=0}^{\pi/2} \frac{2f^2\rho a^2 b^2}{c} |I_m I_n|^2 \sin\theta \, d\theta \, d\phi \tag{29}$$

and

$$|V_{mn}|^2/\Pi_i = \frac{32\rho c |\bar{I}_m \bar{I}_n|^2}{\pi^2 f^2 ab \cos\theta_i m_p^2 \left\{ \left[1 - (f_{mn}/f)^2\right]^2 + (2\zeta f_{mn}/f)^2 \right\}} \tag{30}$$

With these two frequency-response functions, it can be determined whether the modal noise transmission is due more to coupling between the incident noise and the plate vibrations (eq. (30)) or more to coupling of the plate vibrations with the space into which they are radiating (eq. (29)). For the case in which the problem lies with coupling between the incident noise and the plate vibrations, the mean-square velocity divided by incident power can be investigated in terms of the two main quantities which describe its behavior, namely, the mean-square generalized force divided by incident power $\left(|p_{mn}|^2/\Pi_i\right)$ and the plate frequency response divided by incident power $\left(|P_i V_{mn}/p_{mn}|^2/\Pi_i\right)$. The equations governing these two quantities are

$$|p_{mn}|^2/\Pi_i = \frac{128\rho c}{ab\cos\theta_i} |\bar{I}_m \bar{I}_n|^2 \tag{31}$$

and

$$|P_i V_{mn}/p_{mn}|^2/\Pi_i = \frac{2\rho c}{4\pi^2 f^2 m_p^2 ab \cos\theta_i \left\{ [1 - (f_{mn}/f)]^2 + (2\zeta f_{mn}/f)^2 \right\}} \tag{32}$$

The quantity $|p_{mn}|^2/\Pi_i$ indicates how much of the noise transmission is due to the frequency characteristics of the incident noise; the quantity $|P_i V_{mn}/p_{mn}|^2/\Pi_i$ indicates how much of the noise transmission is due to the frequency characteristics of the plate vibrations.

Extension to Midplane Symmetric Composite-Material Plates

The major difference in modeling a midplane symmetric composite plate as opposed to an aluminum plate is that the composite is allowed to be anisotropic. Because of this, the equation of motion shown in equation (1) must be rewritten to account for the anisotropic stiffness terms, resulting in the following equation of motion:

$$D_{11}w_{,\xi\xi\xi\xi} + 4D_{16}w_{,\xi\xi\xi\eta} + 2(D_{12} + 2D_{66})w_{,\xi\xi\eta\eta} + 4D_{26}w_{,\xi\eta\eta\eta} + D_{22}w_{,\eta\eta\eta\eta} + C_D w_{,t} + m_p w_{,tt}$$
$$= p_i(\xi,\eta,t) + p_r(\xi,\eta,t) - p_t(\xi,\eta,t)$$

where a comma denotes the partial differentiation with respect to the subscript and the D_{ij} terms are the anisotropic bending stiffnesses that relate the internal bending and twisting moments of the plate to the twists and curvatures they induce. The theory for calculating the stiffnesses of tape-ply panels is well established (ref. 21), and the values depend on the ply orientation and the stacking sequence. For a simply supported plate, Bert (ref. 22) has calculated an approximate equation for the modal resonant frequencies, and sinusoidal eigenfunctions are used as approximations to the actual mode shapes. With these frequencies and mode shapes, a noise transmission calculation for composite plates can be performed in the same manner as for isotropic plates.

Results of Sample Calculations

Far-Field Transmitted Intensity

In order to carry out the numerical integration in equation (25) to obtain transmitted acoustic power, an understanding of the variation of transmitted intensity is helpful in determining how small a step size is needed to perform the integration. Presented in figures 3 and 4 are sample plots of the effect of frequency on the intensity radiation pattern of a 1.52-m by 1.22-m by 0.081-cm aluminum plate. The results are presented for an incident sound wave at $\theta_i = 45°$ and $\phi_i = 0°$ for two frequencies of 100 Hz and 600 Hz. Figure 3 shows the variation of transmitted intensity with polar angle θ for an azimuthal angle ϕ of 0°. Figure 4 shows the variation of transmitted intensity with azimuthal angle ϕ for a polar angle θ of 45°. These sample results show a trend that was discerned from studying many transmitted-intensity results, that is, as frequency increases, increasingly more of the transmitted sound becomes concentrated at a transmitted angle equal to the incident angle. This results in a steeper variation of intensity with θ and ϕ which, in turn, results in increasingly smaller integration steps being needed as frequency increases. The sample results in figure 4 also display an example of the symmetry which can occur in the transmitted intensity and which helps reduce the numerical integration time. As can be seen in equation (18), with $\phi_i = 0°$ the n-even modes contribute nothing to the transmitted intensity. Thus, in the n-direction of the plate, only the odd modes contribute to the transmitted intensity, and this results in symmetry about $\phi = 0°$. Similarly, for $\phi_i = 90°$, symmetry occurs about $\phi = 90°$; and, for $\phi_i = 0°$, symmetry occurs about both $\phi = 0°$ and $\phi = 90°$. For any other θ_i or ϕ_i, symmetry cannot be shown a priori to occur in the ϕ-direction. An example of this is presented in figure 5, wherein a plot is shown of transmitted intensity variation with ϕ for $\theta = 20°, \theta_i = 60°, \phi_i = 47°$, and $f = 600$ Hz.

For calculating two of the modal components of transmission $\left(\text{i.e.,}\tau_{mn} \text{ and } \Pi_t/|V_{mn}|^2\right)$, numerical integration is required. (See eqs. (28) and (29).) Thus, a detailed investigation of the equation for transmitted intensity was undertaken to determine if any special symmetry occurs for a single mode as opposed to when all the modes are summed. It was found that symmetry occurs about both $\phi = 0°$ and $\phi = 90°$ no matter what the values of θ_i and ϕ_i. This is very helpful information for saving computer time during the numerical integration. An example of this ϕ-direction symmetry for the transmitted intensity of a single mode is presented in figure 6 for $m = 1, n = 11, \theta = 20°, \theta_i = 60°, \phi_i = 47°$, and $f = 600$ Hz.

Transmission Loss

The oblique-incidence transmission loss of a 0.38-m by 0.15-m by 0.081-cm aluminum plate has been calculated for an incident wave at $\theta_i = 60°$ and $\phi_i = 0°$. The results are presented in figure 7 along with a transmission loss calculation based on infinite-panel theory. Although the two curves agree well at high frequency (approximately 2000 Hz and above), for which the panel transmission is the mass-controlled

and coincidence-frequency regions, considerable differences occur at lower frequencies. This is because infinite-panel theory is appropriate only for those high-frequency transmission regions, whereas finite-panel theory is appropriate not only for those regions but also for the low-frequency resonance-controlled and stiffness-controlled transmission regions. Thus, the analytical model developed in this paper is most useful in gaining new insight into the characteristics of noise transmission at low frequency. An example of how the analytical model may be used is shown in figures 8 and 9. In figure 8, transmission loss as a function of polar incidence angle θ_i is shown for two sizes of 0.081-cm-thick aluminum plate, a 0.38-m by 0.15-m plate and a 1.52-m by 1.22-m plate. The azimuthal incidence angle ϕ_i was 0° and the frequency was 600 Hz. The larger panel is slightly more sensitive to θ_i, with about a 5-dB change from $\theta_i = 60°$ to $\theta_i = 0°$. In figure 9 a similar comparison is plotted for transmission loss as a function of ϕ_i with $\theta_i = 45°$ and $f = 600$ Hz. Neither panel is very sensitive to ϕ_i for $\theta_i = 45°$. In both figures, the smaller panel has higher transmission loss because the 600-Hz frequency is within the resonance-controlled transmission region of the smaller panel and within the mass-controlled frequency region of the larger panel.

Modal Decomposition

A demonstration of how the analytical model might be used as a diagnostic tool to gain understanding of a noise transmission problem is presented in this section. The problem, arbitrarily chosen, is the transmission of noise at 600 Hz through a 1.52-m by 1.22-m by 0.081-cm aluminum plate for an incident sound wave at $\theta_i = 60°$ and $\phi_i = 0°$. As a first step, a trial-and-error modal study was done of the transmitted intensity to determine which modes were the largest contributors. The results of this study are summarized in figure 10, in which a plot of the square root of intensity as a function of polar angle θ with $\phi = 0°$ is shown for the total intensity (for all the modes summed together) and for the two largest modal contributors, the $m = 5, n = 1$ mode and the $m = 4, n = 1$ mode. Next, each mode was investigated individually using the modal component equations (28) to (32) to try to determine the specific behavior by which the mode was dominating the transmission. The results of the modal component calculations for the $m = 4, n = 1$ mode are shown in figure 11. In figure 11(a), the ratio of transmitted power to incident power is shown as a function of frequency. The large response near 600 Hz is clearly shown. The graphs of the ratio of transmitted power to mean-square velocity (fig. 11(b)) and of the ratio of mean-square velocity to incident power (fig. 11(c)) show that the high transmission of the plate at 600 Hz for the $m = 4, n = 1$ mode is due more to coupling between the plate vibrations and the acoustic space into which the plate is transmitting than to coupling between the incident sound and the plate vibrations. This coupling on the transmitting side (the peak in fig. 11(b)) occurs at what is commonly referred to as the acoustic short-circuit frequency. This is the minimum frequency for which there is some angle at which the trace wavelength of a transmitted wave will equal the shorter of the two wavelengths of the mode. For all higher frequencies, there will always be an angle for which this wavelength matching will occur, which is why the curve in figure 11(b) flattens out after reaching the short-circuit frequency. In figures 11(d) and 11(e), the breakdown of the ratio of mean-square velocity to incident power into its component parts, namely, the frequency response of the incident noise (fig. 11(d)) and the frequency response of the plate vibrations (fig. 11(e)), is shown and explains the main features of the response in figure 11(c). The peak near 20 Hz in figure 11(c) can be shown in figure 11(e) to be due to the mode's resonant frequency; the peak near 600 Hz in figure 11(c) can be shown to come from a peak in the curve in figure 11(d). The frequency at which these peaks occur is called the coincidence frequency, and it corresponds to the matching of the trace wavelength of the incident sound with the longer of the two wavelengths of the mode. This coupling at the coincidence frequency also contributes to the high transmission at 600 Hz, but it is not as big a contributor as the coupling at the short-circuit frequency.

The results of the modal component calculations for the $m = 5, n = 1$ mode are shown in figures 12(a) to 12(e). Similar results as for the $m = 4, n = 1$ mode are again noted, with the coupling at the short-circuit frequency (fig. 12(c)) playing the major role in the transmission and the coupling at the coincidence frequency (figs. 12(b) and 12(d)) also contributing significantly.

Thus, for the case just discussed, the analytical model facilitates the determination of which modes are dominating the noise transmission and the physical phenomena causing the transmission. The discovery that the physical mechanism involves the matching of wavelengths between the plate and the transmitted noise could be helpful to noise-control engineers. For instance, at least one common method of noise control, plate resonance damping, would be ineffective in this case.

Results for Composite Panels

To further demonstrate the usefulness of the analytical model, sample calculations for two composite panels have been performed to determine the effect of the stacking sequence of the plies on the normal-incidence transmission loss of the panels. The ply material was graphite-epoxy tape. The ply properties were $E_{11} = 137$ GPa, $E_{22} = 10$ GPa, $\nu_{12} = 0.30$, and $G_{12} = 5$ GPa. Each panel was assumed to be made of eight plies layered in a midplane symmetric fashion. One panel, designated as GT1, was assumed to have a symmetric stacking sequence of alternating 0° and 90° plies. The other panel, designated as GT2, was assumed to have a symmetric stacking sequence of alternating 45° and -45° plies. The size of each panel was 0.36 m by 0.20 m by 0.10 cm, with a mass per unit area of 1.59 kg/m^2 and a critical damping ratio of 0.06. The results of the calculations are shown in figure 13. The panel GT2 has a 40-percent increase in fundamental frequency over panel GT1 and thus has a much higher transmission loss in the stiffness-controlled region. At higher frequencies, the curves merge together in the mass-controlled region since both panels have the same weight per unit area.

Concluding Remarks

An improved analytical model has been developed that allows for the efficient calculation of the noise transmission characteristics of a rectangular plate simply supported in an infinite rigid baffle. The governing equations of the analytical model have been derived. Sample calculations comparing the analytical model to infinite-panel theory and showing the usefulness of the analytical model in studying noise transmission have been presented.

Illustrated examples were given of how the model can be used to determine the effect on the transmitted noise of varying the angle of the incident plane wave and to determine far-field directivity of the transmitted noise. Also, examples were given of how the model can be used to determine the modal behavior of a rectangular plate. These included the determination of which modes dominate the noise transmission, the coupling between the incident noise and plate vibrations, the resonance behavior of the plate, and the coupling between the plate vibrations and the transmitted noise.

The applicability of the model to symmetrically layered composite panels has also been demonstrated. Although the analysis approach was developed to study noise transmission into aircraft fuselages, it should be equally applicable to sound transmission through building walls, floors, and windows. Overall, the analytical model was shown to be a versatile and useful tool.

NASA Langley Research Center
Hampton, VA 23665
November 21, 1984

References

1. London, Albert: Transmission of Reverberant Sound Through Single Walls. *J. Res. Nat. Bur. Stand.*, vol. 42, no. 6, June 1949, pp. 605–615.
2. Ordubadi, Afarin; and Lyon, Richard H.: Effect of Orthotropy on the Sound Transmission Through Plywood Panels. *J. Acoust. Soc. America*, vol. 65, no. 1, Jan. 1979, pp. 133–139.

3. Roussos, Louis A.; Grosveld, Ferdinand W.; Koval, Leslie R.; and Powell, Clemans A.: Noise Transmission Characteristics of Advanced Composite Structural Materials. AIAA-83-0694, Apr. 1983.
4. Koval, Leslie R.: *Field-Incidence Transmission of Treated Orthotropic and Laminated Composite Panels.* NASA TM-85680, 1983.
5. Greene, David C.: Vibration and Sound Radiation of Damped and Undamped Flat Plates. *J. Acoust. Soc. America*, vol. 33, no. 10, Oct. 1961, pp. 1315–1320.
6. Wallace, C. E.: Radiation Resistance of a Rectangular Panel. *J. Acoust. Soc. America*, vol. 51, no. 3, pt. 2, Mar. 1962, pp. 946–952.
7. Gomperts, M. C.: Radiation From Rigid Baffled, Rectangular Plates With General Boundary Conditions. *Acustica*, vol. 30, no. 6, June 1974, pp. 320–327.
8. Gomperts, M. C.: Sound Radiation From Baffled, Thin, Rectangular Plates. *Acustica*, vol. 37, no. 2, Mar. 1977, pp. 93–102.
9. Nigam, S. P.; Grover, G. K.; and Lal, S.: Sound Radiation From a Simply Supported Rectangular Plate Vibrating Under Complex Modes. *Israel J. Technol.*, vol. 15, no. 3, 1977, pp. 123–129.
10. Shen, Y.; and Oldham, D. J.: Sound Radiation From Building Elements. *J. Sound & Vib.*, vol. 84, no. 1, Sept. 8, 1982, pp. 11–33.
11. Lomas, N. S.; and Hayek, S. I.: Vibration and Acoustic Radiation of Elastically Supported Rectangular Plates. *J. Sound & Vib.*, vol. 52, no. 1, May 8, 1977, pp. 1–25.
12. Young, James E.: Transmission of Sound Through Thin Elastic Plates. *J. Acoust. Soc. America*, vol. 26, no. 4, July 1954, pp. 485–492.
13. Eichler, E. G.; and Lambert, R. F.: Acoustic (0, 1) Wave Transmission Through Thin Rectangular Plates. *Acustica*, vol. 7, no. 6, 1957, pp. 379–386.
14. Sewell, E. C.: Transmission of Reverberant Sound Through a Single-Leaf Partition Surrounded by an Infinite Rigid Baffle. *J. Sound & Vib.*, vol. 12, no. 1, May 1970, pp. 21–32.
15. Tohyama, M.; and Itow, T.: Theoretical Interpretation of the Mass Law Based on the Wave Theory. *Acustica*, vol. 30, no. 1, Jan. 1974, pp. 1–11.
16. Guyader, J. L.; and Lesueur, C.: Acoustic Transmission Through Orthotropic Multilayered Plates, Part II: Transmission Loss. *J. Sound & Vib.*, vol. 58, no. 1, May 8, 1978, pp. 69–86.
17. Kinsler, Lawrence E.; and Frey, Austin R.: *Fundamentals of Acoustics*, Second ed. John Wiley & Sons, Inc., c.1962.
18. Myint-U, Tyn: *Partial Differential Equations of Mathematical Physics*, Second ed. Elsevier Science Pub. Co., Inc., c.1980.
19. Pierce, Allan D.: *Acoustics—An Introduction to Its Physical Principles and Applications.* McGraw-Hill, Inc., c.1981.
20. Gerald, Curtis F.: *Applied Numerical Analysis*, Second ed. Addison-Wesley Pub. Co., c.1978.
21. Jones, Robert M.: *Mechanics of Composite Materials.* Scripta Book Co., c.1975.
22. Bert, C. W.: Optimal Design of a Composite-Material Plate To Maximize Its Fundamental Frequency. *J. Sound & Vib.*, vol. 50, no. 2, Jan. 22, 1977, pp. 229–237.

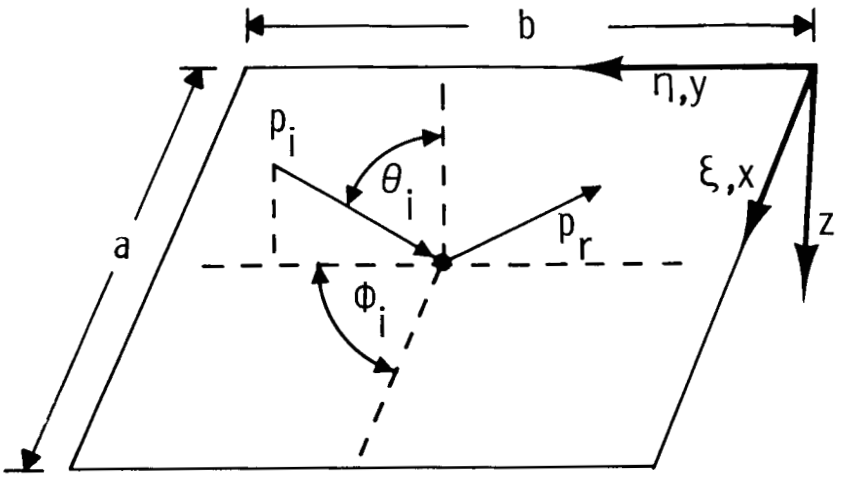

Figure 1. Geometry on incident side of plate.

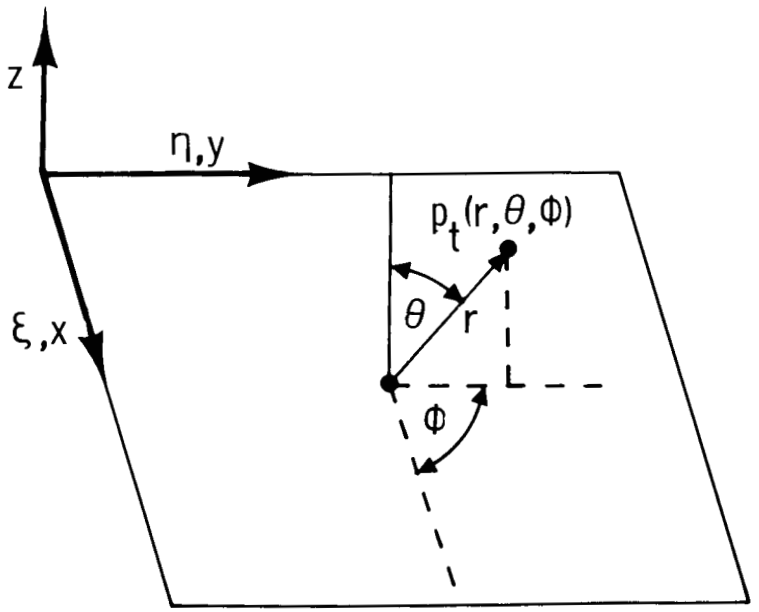

Figure 2. Geometry on radiating side of plate.

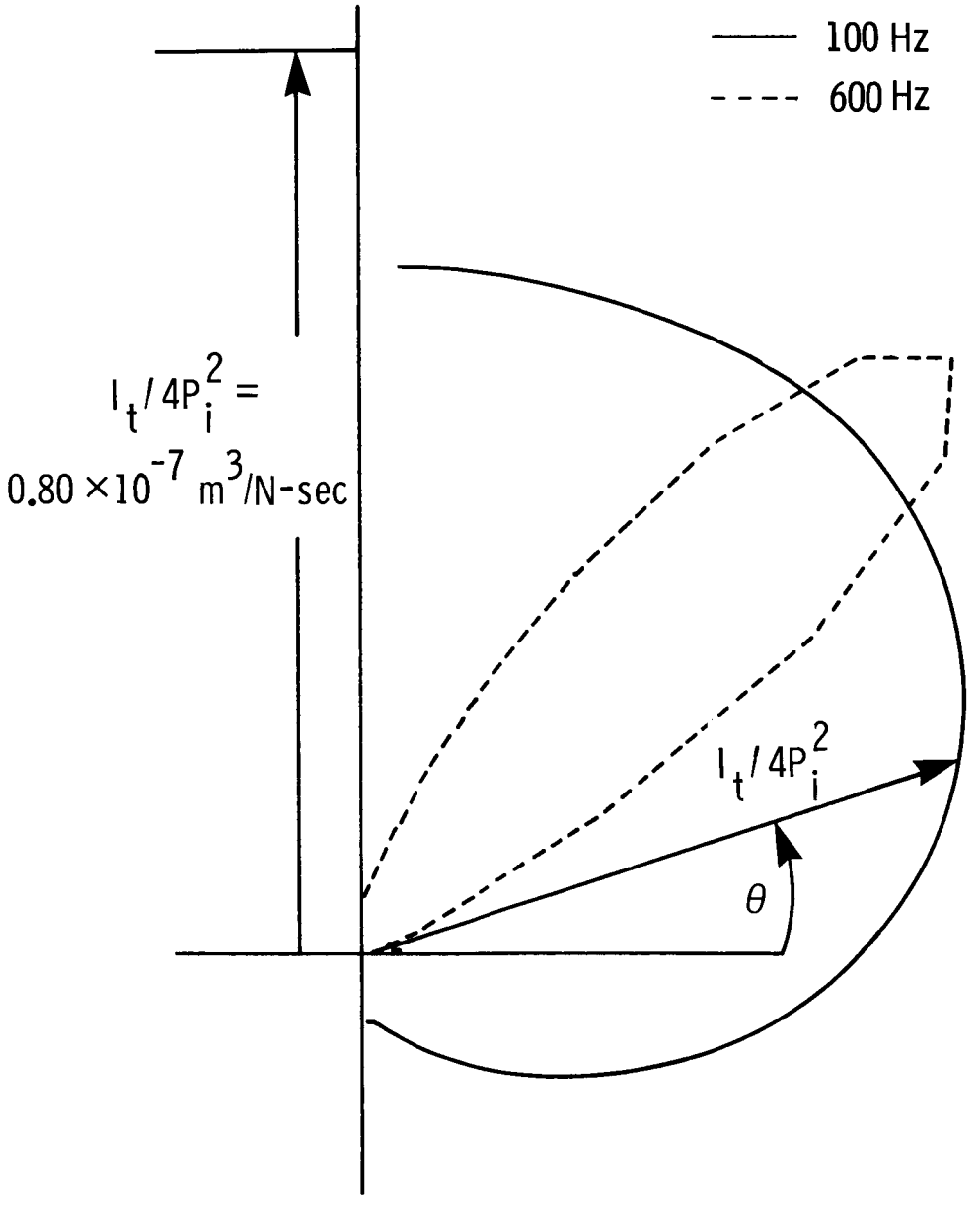

Figure 3. Transmitted-intensity variation in θ-direction for 1.52-m by 1.22-m by 0.081-cm aluminum plate. $\theta_i = 45°$; $\phi_i = 0°$; $\phi = 0°$.

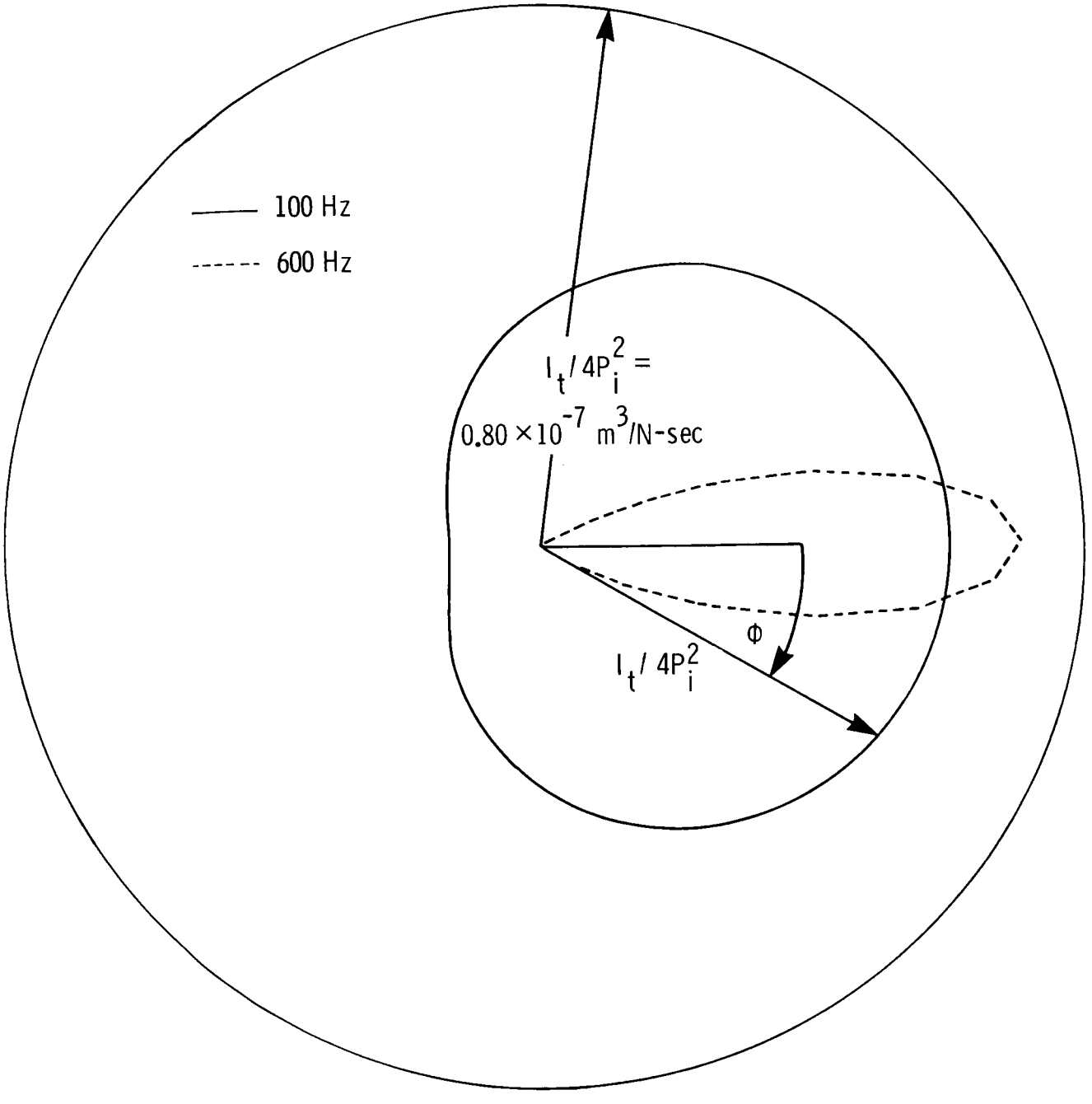

Figure 4. Transmitted-intensity variation in ϕ-direction for 1.52-m by 1.22-m by 0.081-cm aluminum plate. $\theta_i = 45°$; $\phi_i = 0°$; $\theta = 45°$.

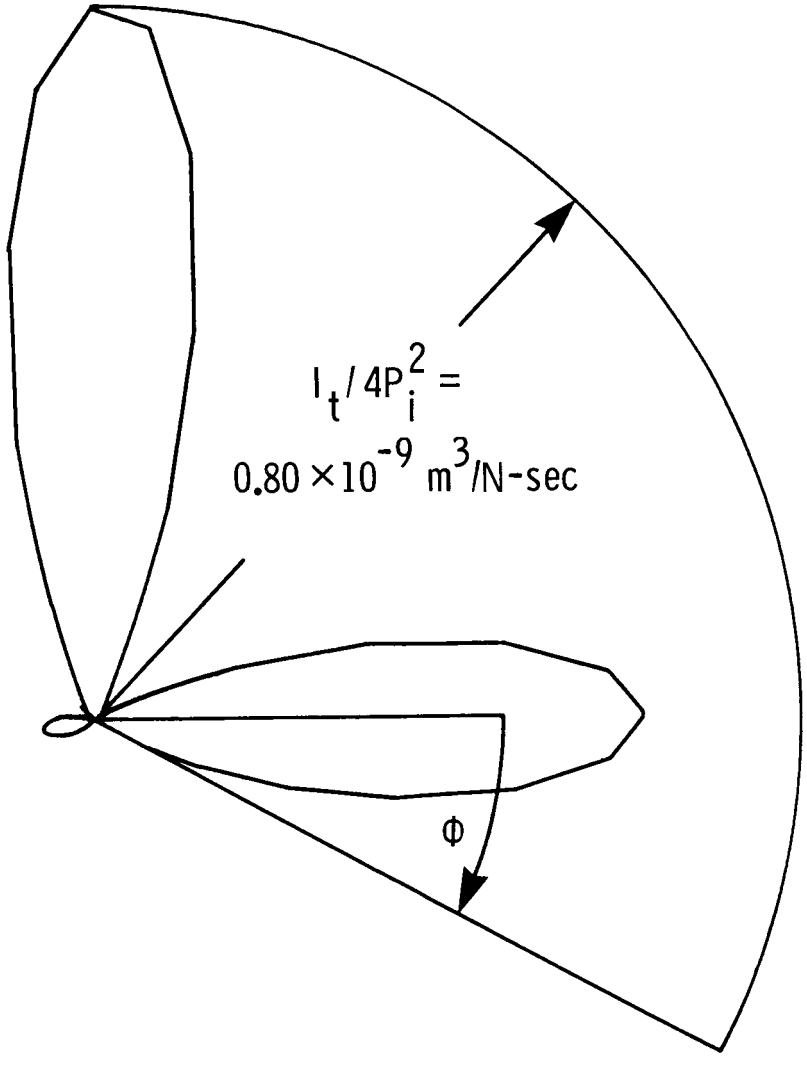

Figure 5. Transmitted-intensity variation in ϕ-direction for 1.52-m by 1.22-m by 0.081-cm aluminum plate for $f = 600$ Hz. $\theta_i = 60°$; $\phi_i = 47°$; $\theta = 20°$.

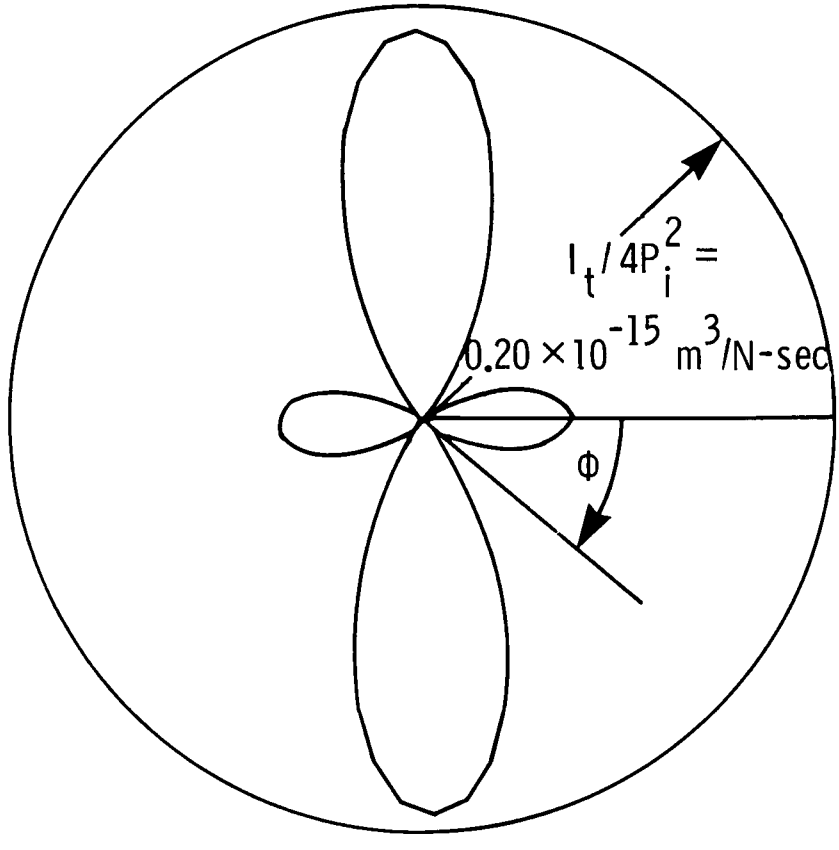

Figure 6. Transmitted-intensity variation in ϕ-direction for 1.52-m by 1.22-m by 0.081-cm aluminum plate for $m = 1$, $n = 11$, and $f = 600$ Hz. $\theta_i = 60°$; $\phi_i = 47°$; $\theta = 20°$.

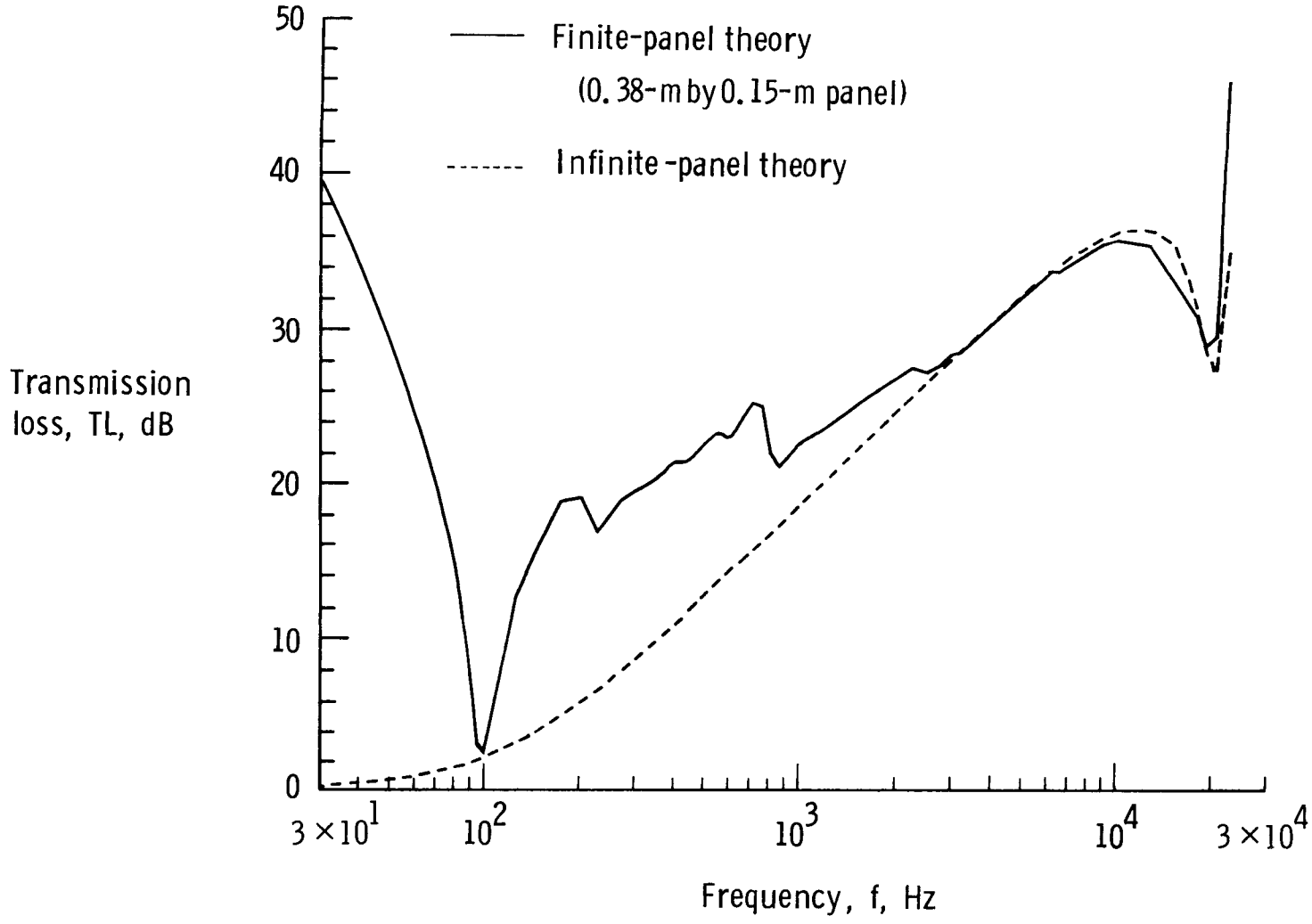

Figure 7. Finite-panel-theory and infinite-panel-theory calculations of oblique-incidence transmission loss for 0.081-cm-thick aluminum panel. $\theta_i = 60°$; $\phi_i = 0°$.

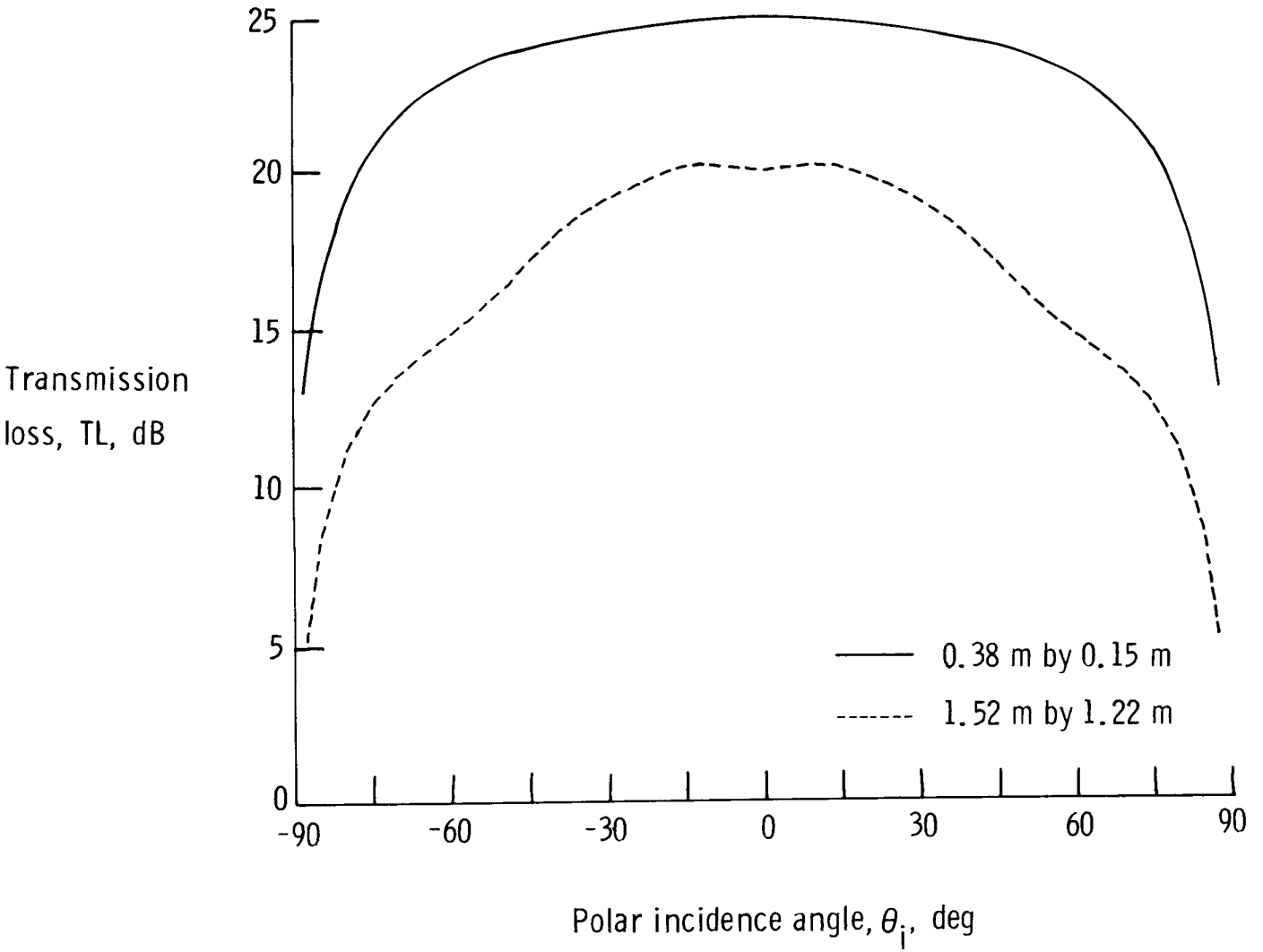

Figure 8. Variation of transmission loss with polar incidence angle θ_i for two 0.081-cm-thick aluminum plates. $\phi_i = 0°$; $f = 600$ Hz.

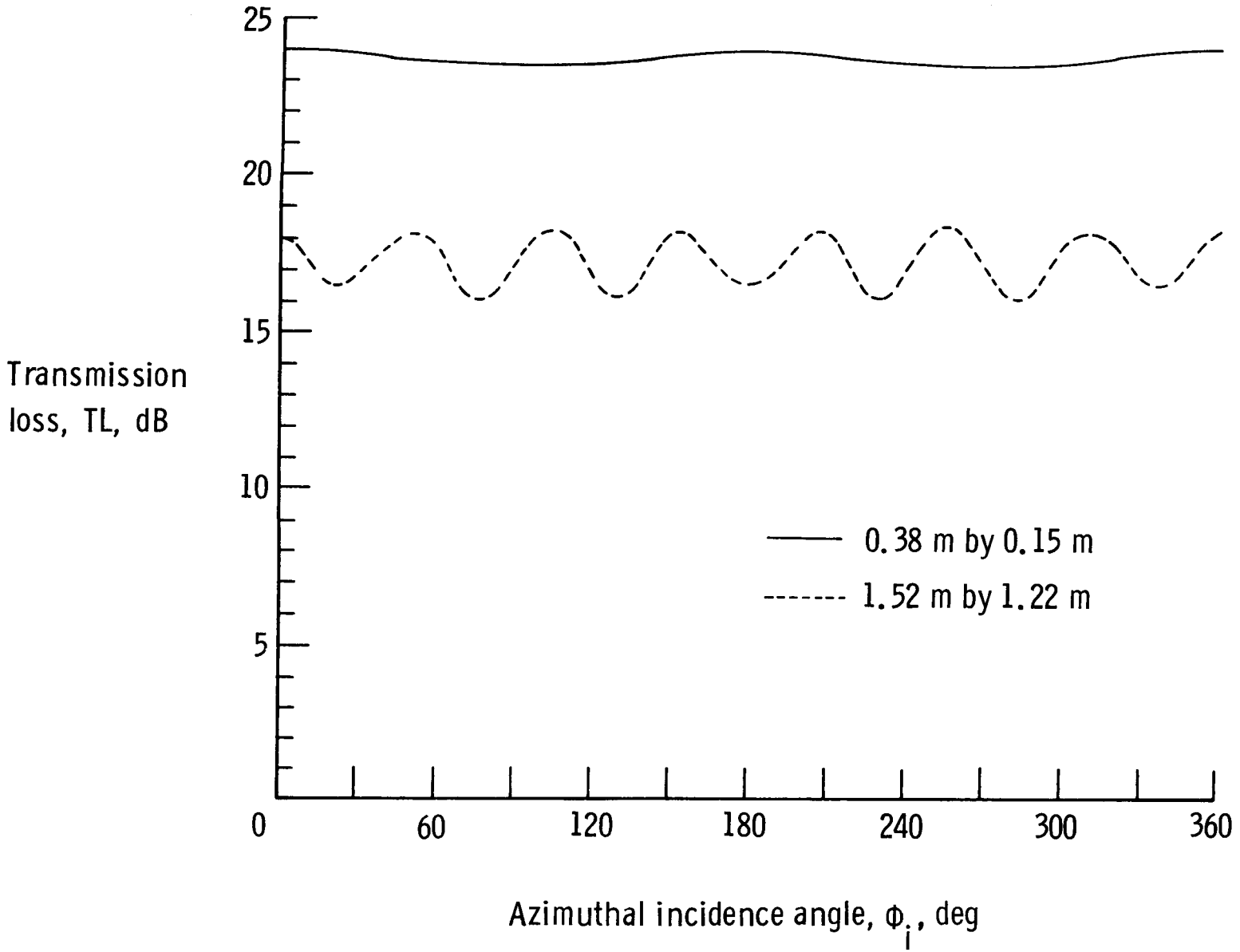

Figure 9. Variation of transmission loss with azimuthal incidence angle ϕ_i for two 0.081-cm-thick aluminum plates. $\theta_i = 45°$; $f = 600$ Hz.

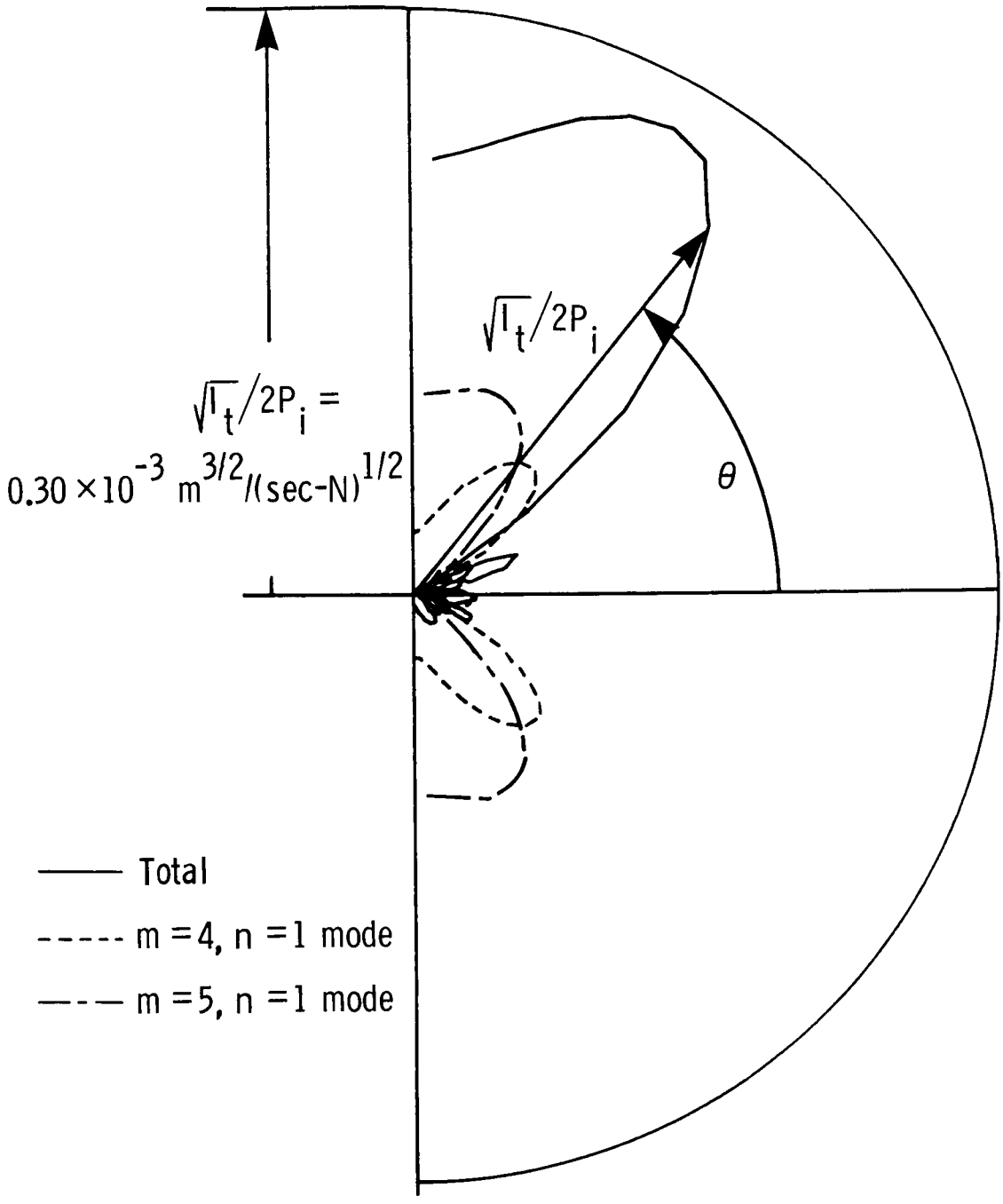

Figure 10. Variation of square root of transmitted intensity in θ-direction for 1.52-m by 1.22-m by 0.081-cm aluminum plate. $\theta_i = 60°$; $\phi_i = 0°$; $\phi = 0°$; $f = 600$ Hz.

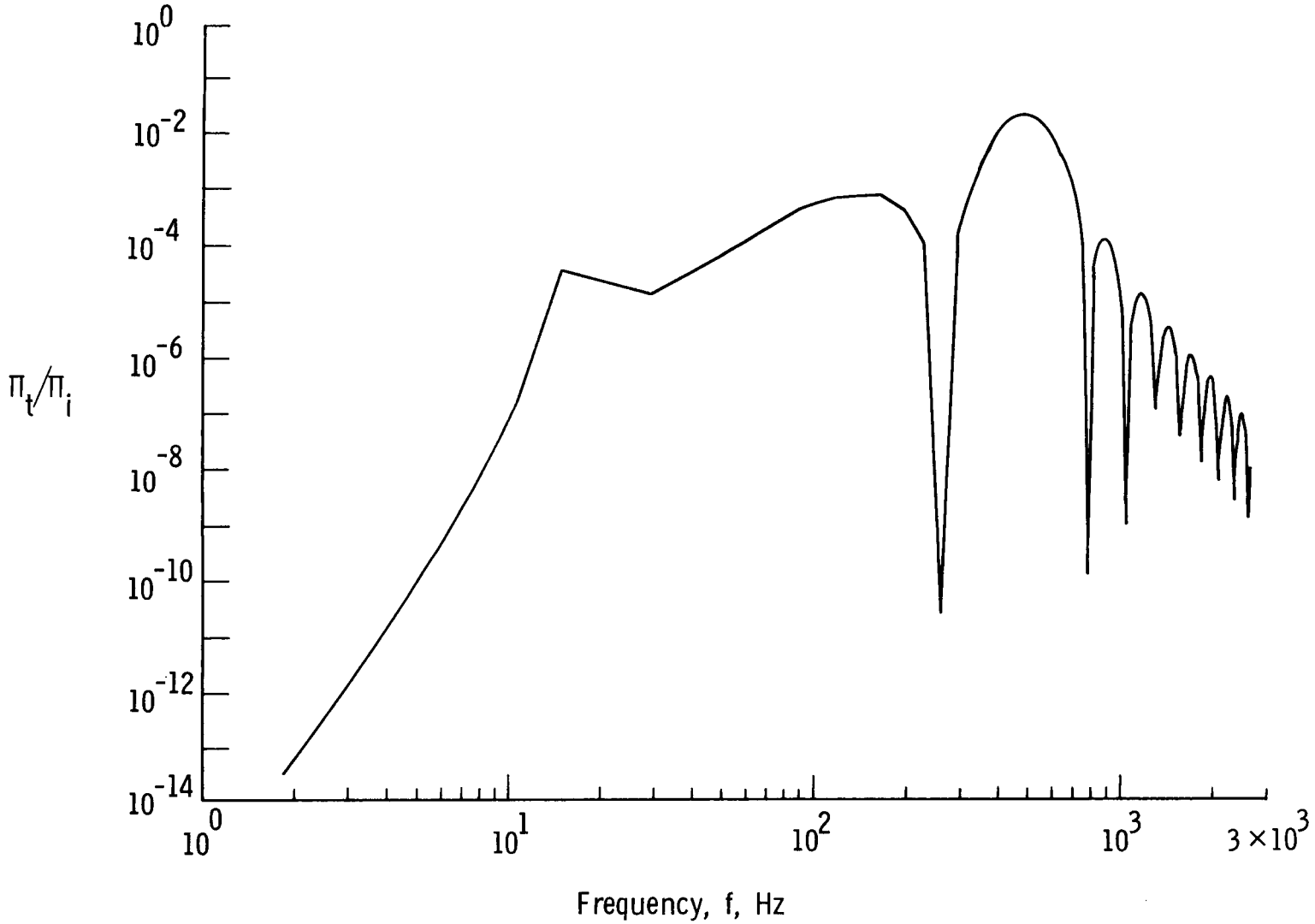

(a) Ratio of transmitted power to incident power.

Figure 11. Noise transmission response curves for $m = 4$, $n = 1$ mode of a 1.52-m by 1.22-m by 0.081-cm aluminum plate. $\theta_i = 60°$; $\phi_i = 0°$.

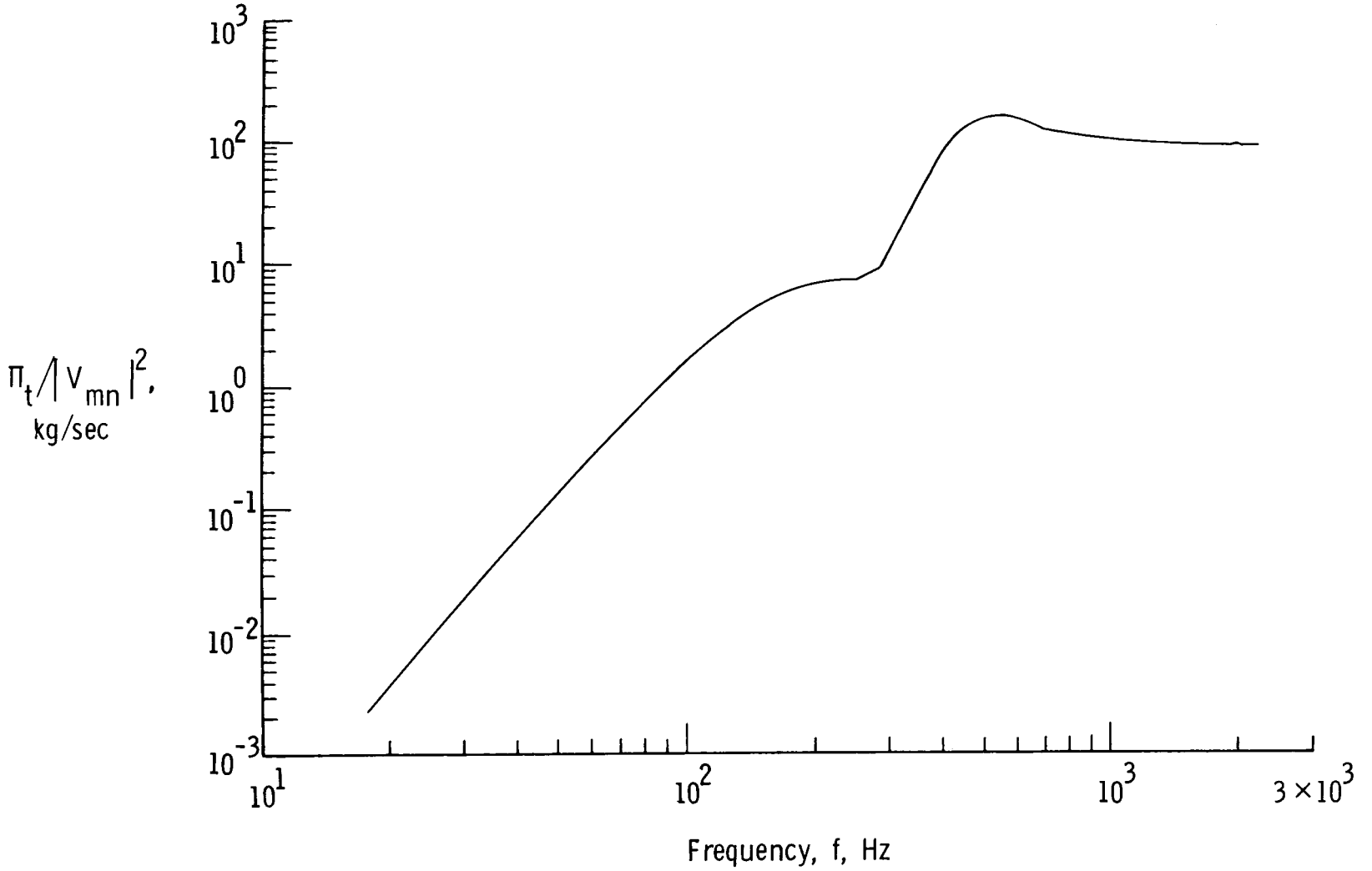

(b) Ratio of transmitted power to mean-square plate velocity.

Figure 11. Continued.

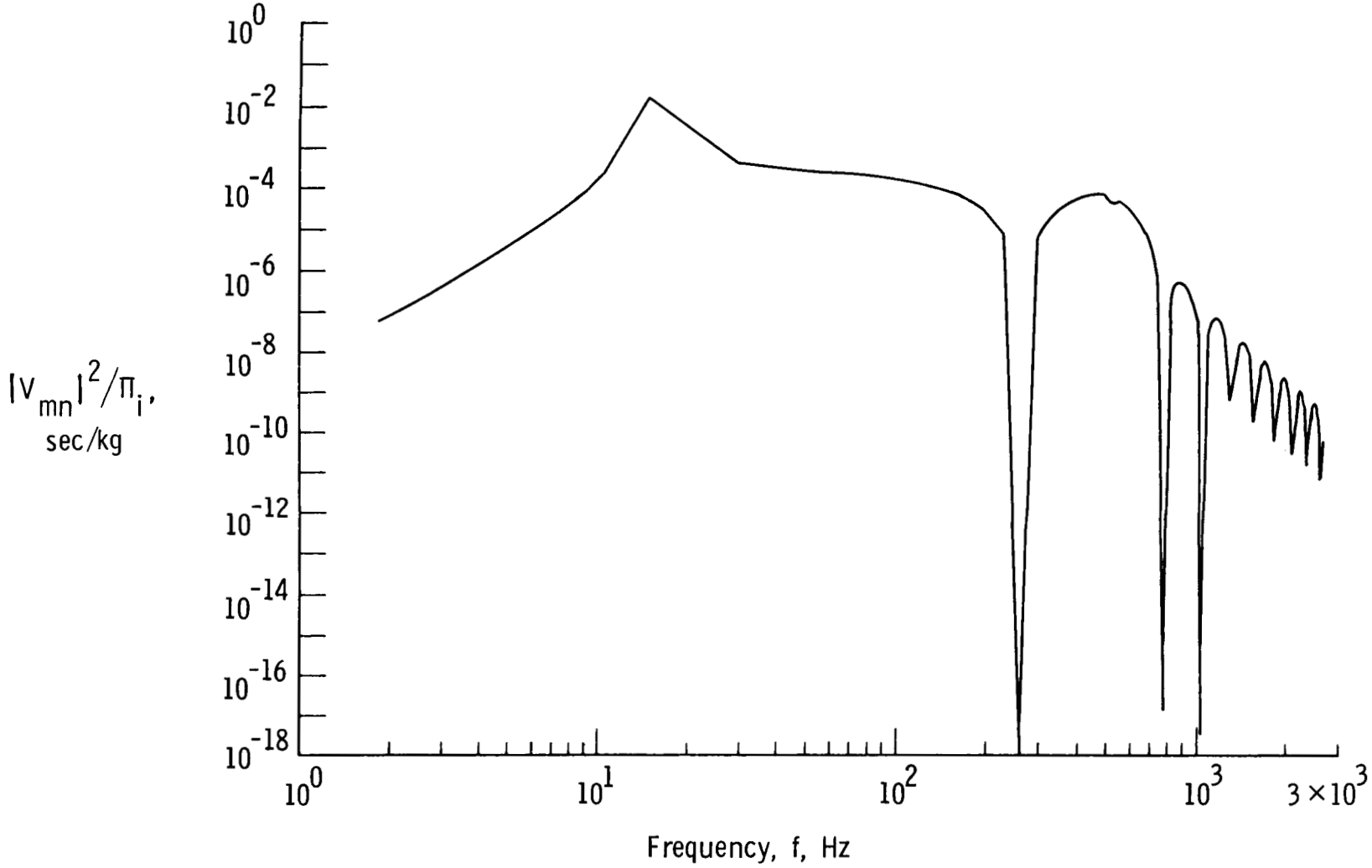

(c) Ratio of mean-square plate velocity to incident power.

Figure 11. Continued.

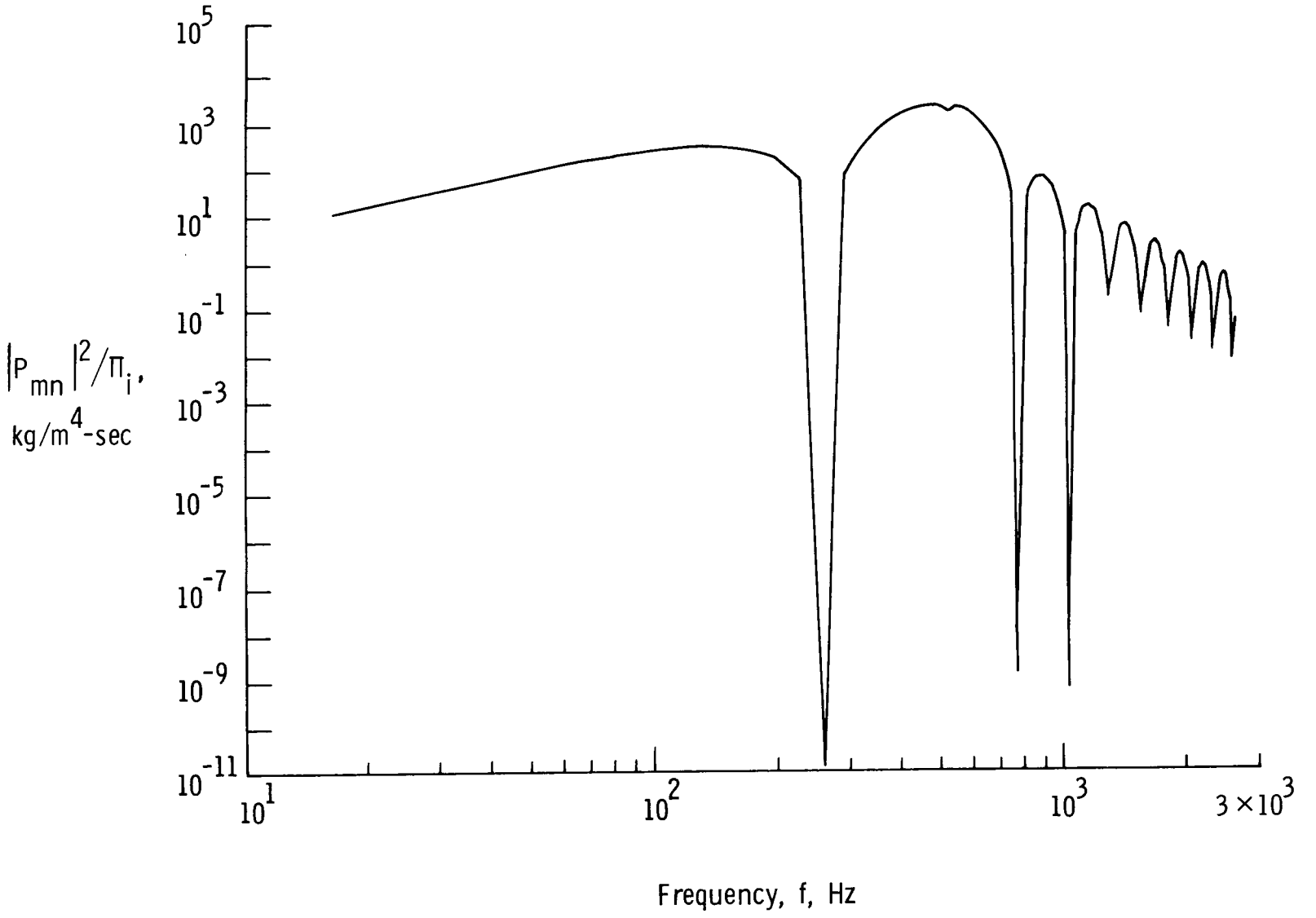

(d) Ratio of mean-square generalized force to incident power.

Figure 11. Continued.

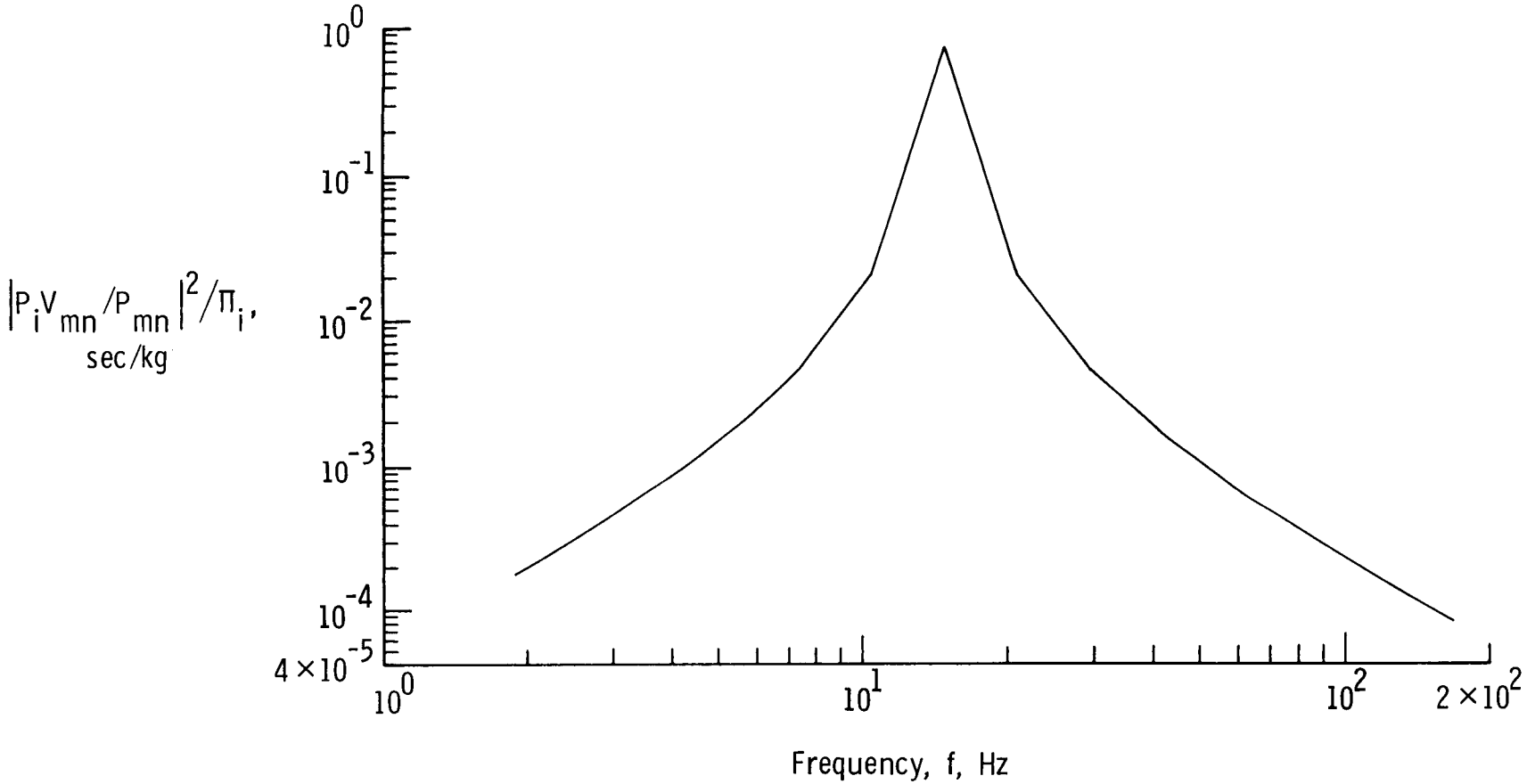

(e) Ratio of plate frequency response to incident power.

Figure 11. Concluded.

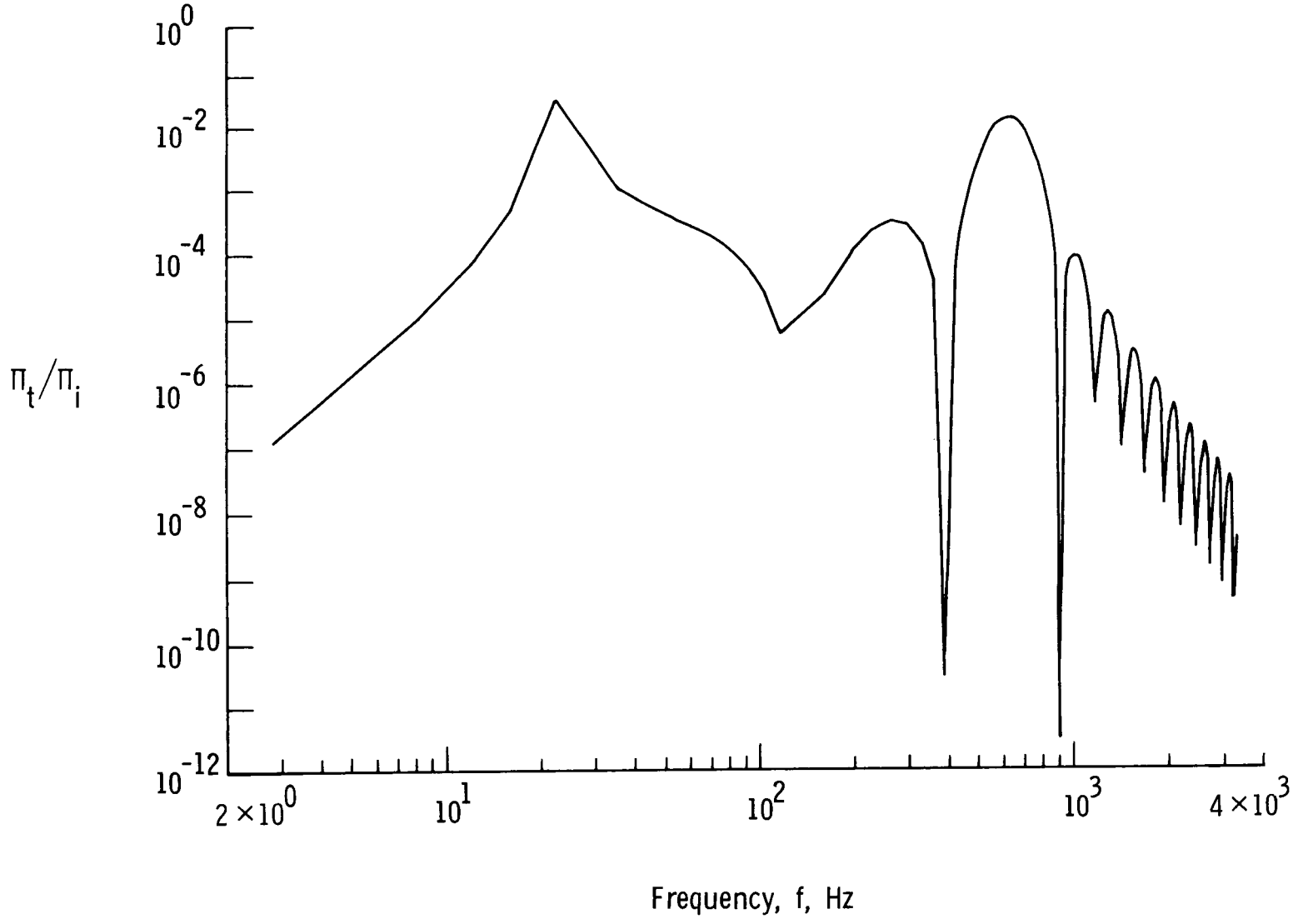

(a) Ratio of transmitted power to incident power.

Figure 12. Noise transmission response curves for $m = 5$, $n = 1$ mode of a 1.52-m by 1.22-m by 0.081-cm aluminum plate. $\theta_i = 60°$; $\phi_i = 0°$.

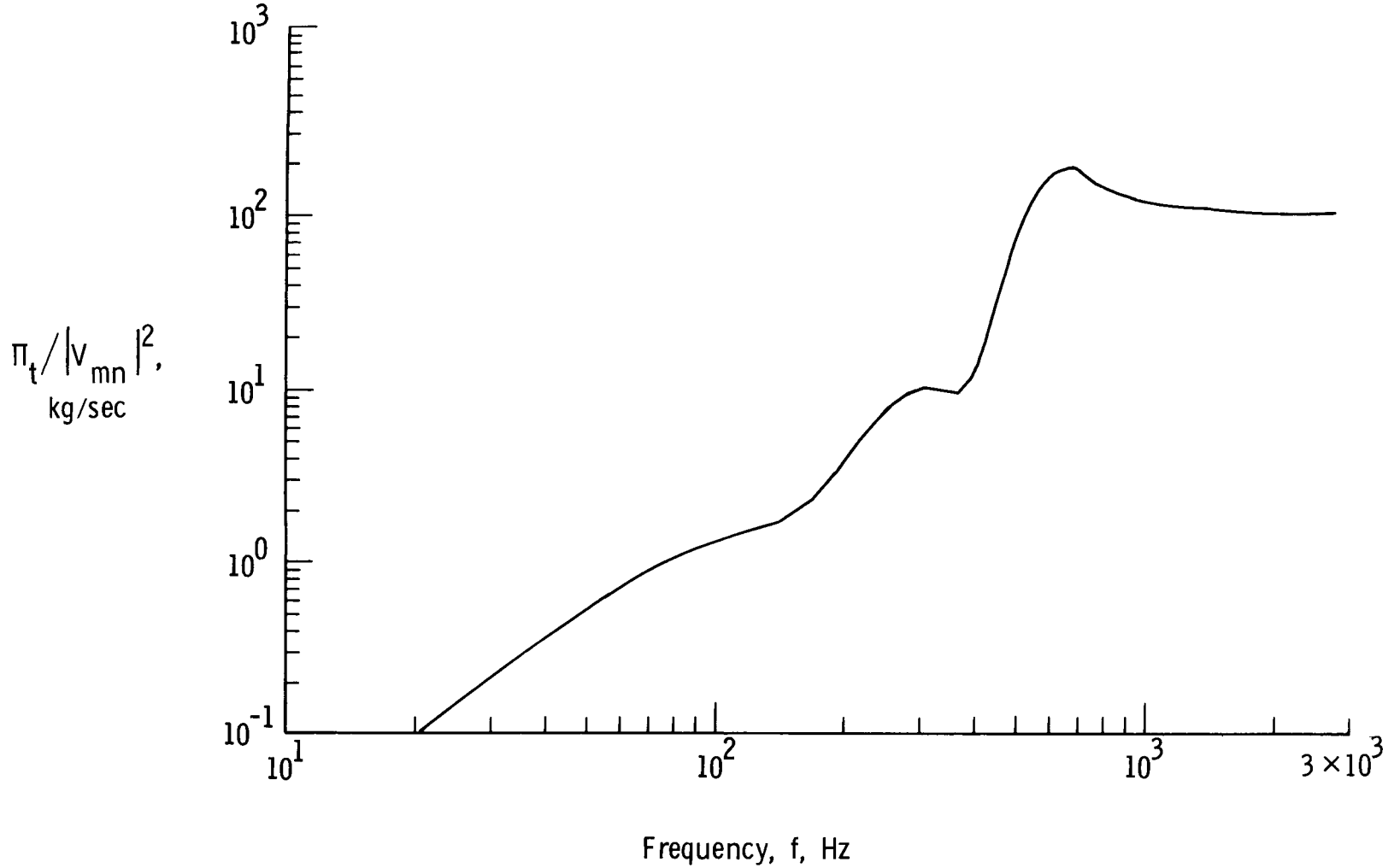

(b) Ratio of transmitted power to mean-square plate velocity.

Figure 12. Continued.

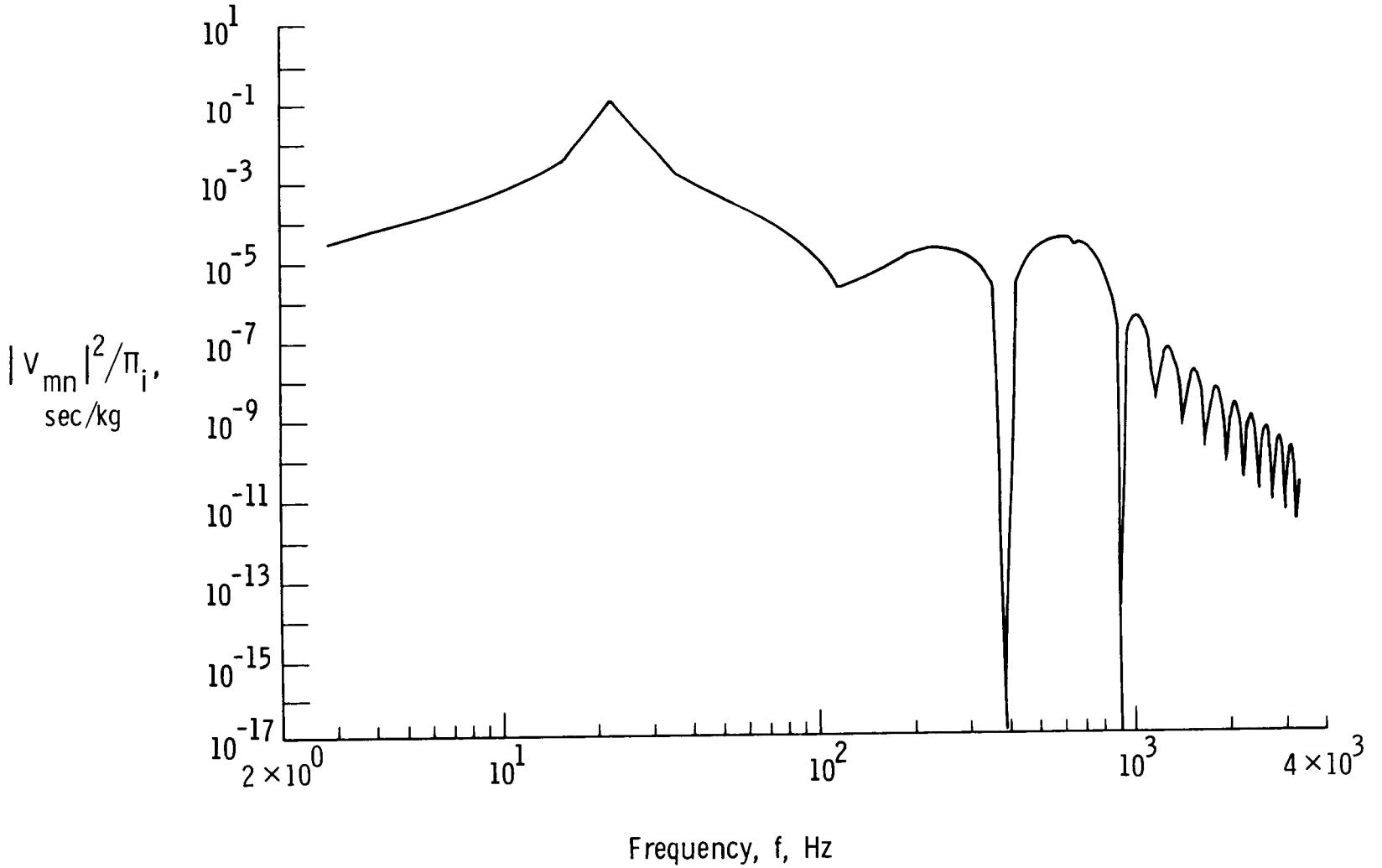

(c) Ratio of mean-square velocity to incident power.

Figure 12. Continued.

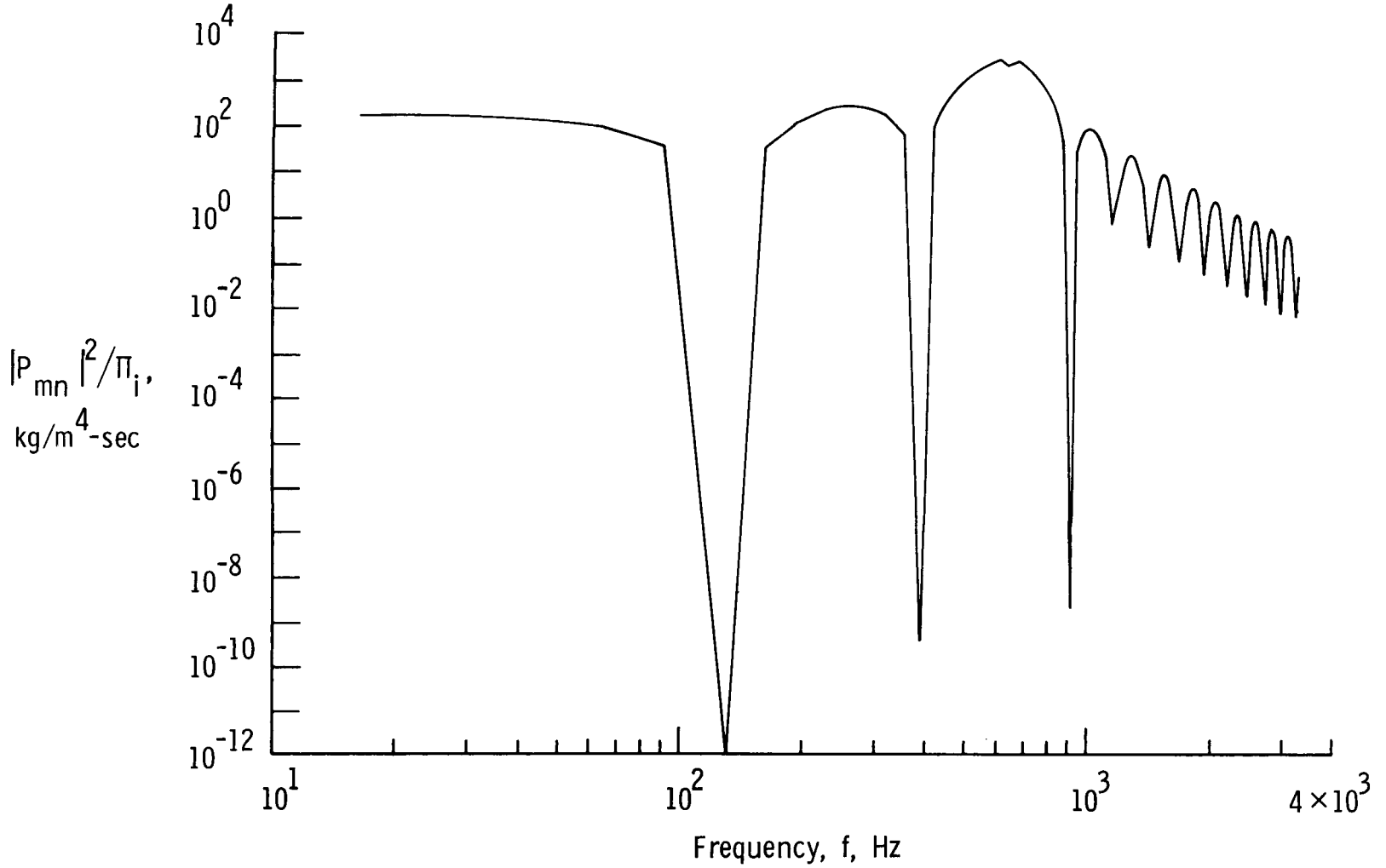

(d) Ratio of mean-square generalized force to incident power.

Figure 12. Continued.

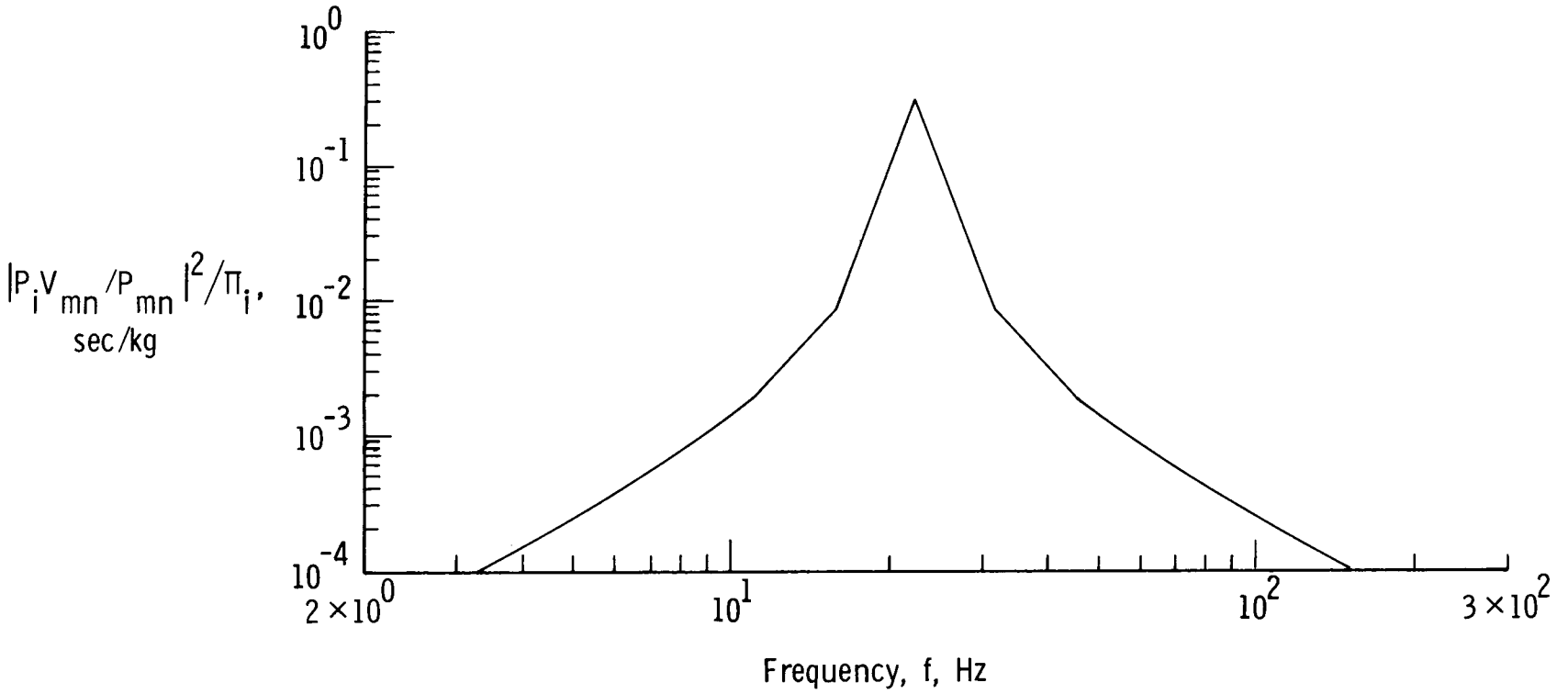

(e) Ratio of plate frequency response to incident power.

Figure 12. Concluded.

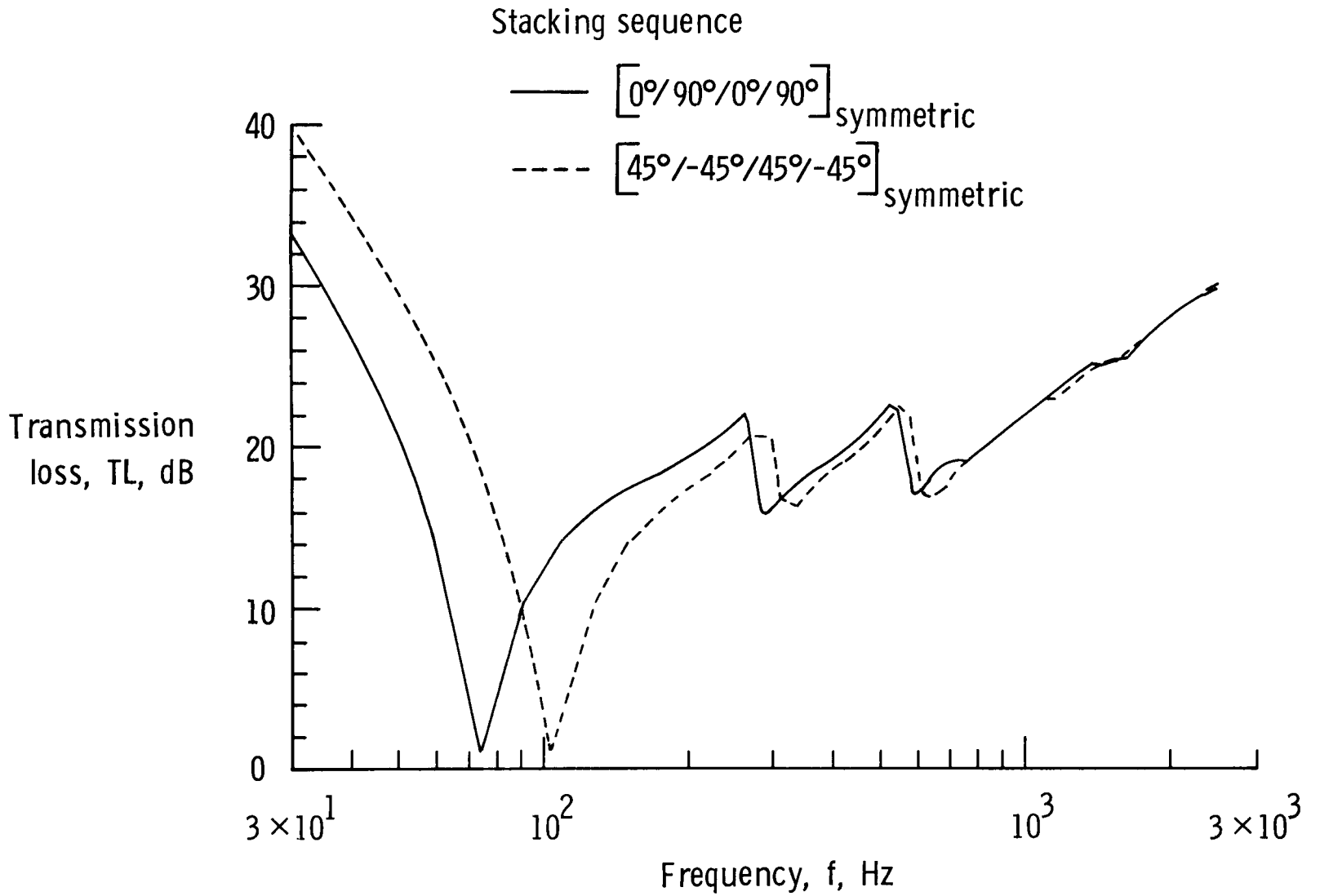

Figure 13. Transmission loss calculations for two graphite-epoxy composite panels having equal mass but different fiber orientations and stacking sequences. $\theta_i = 0°$; $\phi_i = 0°$; $a = 0.36$ m; $b = 0.20$ m; Thickness = 0.10 cm.

1. Report No.	2. Government Accession No.	3. Recipient's Catalog No.
NASA TP-2398		

4. Title and Subtitle	5. Report Date
Noise Transmission Loss of a Rectangular Plate in an Infinite Baffle	March 1985
	6. Performing Organization Code: 505-33-53-03
7. Author(s): Louis A. Roussos	8. Performing Organization Report No.: L-15861
9. Performing Organization Name and Address: NASA Langley Research Center, Hampton, VA 23665	10. Work Unit No.
	11. Contract or Grant No.
12. Sponsoring Agency Name and Address: National Aeronautics and Space Administration, Washington, DC 20546	13. Type of Report and Period Covered: Technical Paper
	14. Sponsoring Agency Code

15. Supplementary Notes

Presented at the 107th Meeting of the Acoustical Society of America held on May 7-10, 1984, in Norfolk, Virginia.

16. Abstract

An improved analytical procedure has been developed that allows for the efficient calculation of the noise transmission characteristics of a finite rectangular plate. Both isotropic and symmetrically laminated composite plates are considered. The plate is modeled with classic thin-plate theory and is assumed to be simply supported on all four sides. The incident acoustic pressure is assumed to be a plane wave impinging on the plate at an arbitrary angle. The reradiated pressure is assumed to be negligible compared with the blocked pressure, and the plate vibrations are calculated by a normal-mode approach. A Green's function integral equation is used to link the plate vibrations to the transmitted far-field sound waves, and transmission loss is calculated from the ratio of incident to transmitted acoustic powers. The result is a versatile research and engineering analysis tool that not only predicts noise transmission loss but also enables the determination of the modal behavior of the plate.

17. Key Words (Suggested by Authors(s))	18. Distribution Statement
Noise transmission Transmission loss Finite plate Composite materials	Unclassified—Unlimited Subject Category 71

19. Security Classif.(of this report)	20. Security Classif.(of this page)	21. No. of Pages	22. Price
Unclassified	Unclassified	34	A03

For sale by the National Technical Information Service, Springfield, Virginia 22161

NASA-Langley, 1985

5 2 1U,H, 850322 S00161DS
DEPT OF THE AIR FORCE
ARNOLD ENG DEVELOPMENT CENTER(AFSC)
ATTN: LIBRARY/DOCUMENTS
ARNOLD AF STA TN 37389